COMPRESSION AND RECONSTRUCTION OF

HADAMARD NATURALNESS-PRESERVING

TRANSFORM CODED IMAGES

By

CHARLOTTE R. FORE

Bachelor of Science
Oral Roberts University
Tulsa, Oklahoma
1989

Master of Science
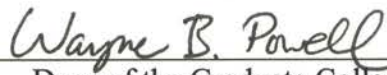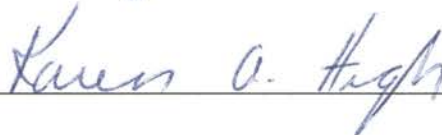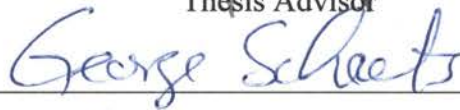Oklahoma State University
Stillwater, Oklahoma
1993

Submitted to the Faculty of the
Graduate College of the
Oklahoma State University
in partial fulfillment of
the requirements for
the Degree of
DOCTOR OF PHILOSOPHY
May, 1999

COMPRESSION AND RECONSTRUCTION OF

HADAMARD NATURALNESS-PRESERVING

TRANSFORM CODED IMAGES

Thesis Approved:

_____
Thesis Advisor

_____
George Scheets

_____
Karen A. High

_____
K. A. Tym

_____
Wayne B. Powell
Dean of the Graduate College

ii

ACKNOWLEDGMENTS

I would like to thank my thesis advisor, Dr. Rao Yarlagadda, for his technical guidance and patience throughout this project. His support, friendship, and technical expertise paved the way for the successful completion of this thesis. I would like to thank Dr. Karen High, Dr. George Scheets, and Dr. Keith Teague for serving on my oral examination committee.

Additionally, I owe a great debt of thanks to my family. Their constant encouragement, prayers, and support made this thesis possible. I want to give special thanks to my husband, Kirk Fore, for his supportive efforts during all the years of my studies and his helpful comments and proofreading. I also thank my son, Ian, for his patience and for making my life much more colorful.

TABLE OF CONTENTS

LIST OF TABLES

LIST OF FIGURES

ACRONYMS

AAL	ATM Adaptation Layer
ATM	Asynchronous Transfer Mode
DCT	Discrete Cosine Transform
DPCM	Differential Pulse Code Modulation
HNPT	Hadamard Naturalness-Preserving Transform
JPEG	Joint Photographic Experts Group
KLT	Karhunen-Loeve Transform
KS	Kolmogorov-Smirnov
LM	Lloyd-Max
MPEG	Motion Pictures Experts Group
NPT	Naturalness-Preserving Transform
POCS	Projections Onto Convex Sets
PSNR	Peak Signal-to-Noise Ratio
QMF	Quadrature Mirror Filter
SNR	Signal-to-Noise Ratio
UTQ	Uniform Threshold Quantizer

CHAPTER 1

INTRODUCTION

As the number of multimedia applications and products increases, image compression techniques continue to be important tools for the efficient storage and transmission of gray-scale and color images. Image coders fall into one of two general categories: transform based coders or subband coders. Orthogonal transforms such as the Discrete Cosine Transform (DCT) are typically used in popular compression algorithms because of their good energy compaction properties and their ability to decorrelate the image data well. The availability of fast computation algorithms also contribute to the wide use of standard transform-based compression algorithms like JPEG (Joint Photographic Experts Group) [19] [35] and MPEG (Motion Pictures Experts Group) [20]. Subband (or wavelet) coders [15] [45] [50] are another popular method for compressing image data. By cascading horizontal and vertical two band filter banks, subband coding provides a scalable or multiresolution image representation.

Most algorithms in digital image compression focus on achieving high signal-to-noise ratios at high compression ratios. Transmission of data over a communications channel frequently results in the loss or corruption of the original data. This loss can be due to noise, network congestion, signal degradation, jamming, etc. Another source of loss is the compression algorithm used at the encoder. A hybrid transform was proposed

by Yarlagadda and Hershey in [54] and [55] for possible use in situations where the communications channel results in severely degraded output images. The Hadamard Naturalness-Preserving Transform (HNPT) of an image contains some of the features of the original image while other transform coefficient characteristics are the result of the Hadamard portion of the transform.

This thesis describes an image coding system which focuses on both the compression of HNPT data and the restoration of images received from corrupted HNPT data. The techniques presented look at all three aspects of the data transmission problem: compression of image data, lossy transmission, and restoration and error concealment in the received images. The error concealment technique presented differs from conventional error detection/correction methods such as Hamming codes and is implemented at the decoder. The algorithms described in the following chapters are well suited to a communications channel with limited bandwidth and with computational power available at the decoder.

In order to generate low bit rate output, image coders remove redundancy and transmit a reduced data set. DCT-based coders divide an image into small blocks, decorrelate the data with their selected transform, discard high-frequency transform coefficients, quantize remaining coefficients, and finally entropy encode the data to be sent to the decoder. Subband coders split the original image's frequency band into smaller non-overlapping frequency bands. The subbands can be encoded independently using either pdf optimized quantizers [48] or uniform threshold quantizers [15] [45]. Vector quantization techniques have also been used to take advantage of the correlation between subband samples in the different subbands [47][48]. To achieve moderate

compression ratios, a number of the less important transform/subband coefficients are discarded and the overall image context is preserved with some loss of detail. To achieve high compression ratios, a greater number of transform/subband coefficients are discarded resulting in lower quality decoded images.

Distortion is a measure of the quality of a compressed representation of the image. Mean square error (MSE) is the most commonly used distortion measure. For N pixels,

$$MSE = \frac{1}{N} \sum_{i=o}^{N-1} |x_i - \hat{x}_i|^2 \tag{1.1}$$

where the x_i's are the input signal values and $\hat{x}_i$'s are the reconstructed signal values. MSE provides a measure of the error between the original signal and the signal reconstructed from the compressed representation. Signal-to-noise ratio (SNR) and peak signal-to-noise ratio (PSNR) are also MSE based distortion metrics

$$SNR = 10 \log_{10} \frac{\sigma^2}{MSE} \tag{1.2}$$

$$PSNR = 10 \log_{10} \frac{M^2}{MSE} \tag{1.3}$$

where σ^2 is the signal variance and M is the maximum peak value in the input signal. For 8 bit grayscale images M has a value of 255. Although these quantitative distortion measures are widely used because of their ease of implementation, they are not necessarily good indicators of visual quality.

At high compression ratios the image data is coarsely approximated and distortion is inevitable. The three main types of distortion are classified either as blurring, blocking, or ringing artifacts. Blurring results from the loss of high frequency information during quantization and occurs in both transform and subband coded images.

The blocking artifact is the most noticeable artifact of low bit rate JPEG compression. The discontinuities between boundaries of adjacent blocks are a natural consequence of the independent processing of each block. On the other hand, low bit rate subband coded images suffer from ringing artifacts near sharp edges.

In some cases, the goal of a good image compression algorithm can be redefined as preserving image features that are important to the user and reducing any undesirable distortions from compression of the data. As an example, the human visual system has more sensitivity to edge distortion in an image than to high noise levels [18]. In flat, smooth regions of an image, the human observer has a lower contrast sensitivity [3]. For this reason a visually pleasing restored image may not always be the most accurate reconstruction (high PSNR). Medical imaging is another area where large blocks of storage space are required to store the data. A typical MRI image contains 256x256x12 pixels. Loss of valuable details and other image information could lead to a wrong diagnosis. Current biomedical imaging programs [28] allow the user to select which regions of the image are to be preserved with little or no compression.

The theory of projections onto convex sets (POCS) has been suggested [42] [51] to improve the quality of JPEG compressed images. POCS provides an iterative method for restoring a representation of the original image from partial image data. *A priori* knowledge about characteristics of the original image is used along with the received image to reconstruct an estimate of the original. Some examples of *a priori* knowledge are image smoothness, i.e. no blocking artifacts, and valid pixel intensities.

Iterative restoration techniques similar to POCS have been successfully used with the HNPT to restore data that is lost due to errors in the communications channel [31]

[32] [33][54]. In [54], the reconstruction algorithm was designed with two considerations in mind. First, many tactical images have large regions of a known background texture such as a clear sky. Texture is a spatial property that can be described in terms of qualitative measures such as smoothness, coarseness, and periodicity of image features. Secondly, for images where large contiguous portions of the transmitted data are lost, a human operator can identify these regions and substitute a texture estimate for the missing pixels.

There are two useful aspects of the HNPT which should be noted. First is the computational complexity of performing the transform. The HNPT of an image can be constructed using only additions and subtractions. Second, the HNPT is a closed, convex function. Since fast algorithms are available for computing the Hadamard transform [44][54], using the HNPT in conjunction with a convex set based restoration scheme is feasible.

The remainder of this thesis is organized as follows. In Chapter 2 the HNPT is formally defined and statistical properties of HNPT coded images are discussed. Chapter 3 provides an overview of the image compression, transmission, and reconstruction processes. This chapter introduces the basic algorithms for both transform coding and subband coding of images. Also included is a discussion of the image restoration problem and POCS based image recovery techniques. Network assumptions for packet-based image transmission are presented. Chapter 4 discusses histogram modeling and quantization issues. Quantizers designed specifically for use in compressing the HNPT coefficients are presented along with image compression results. Chapter 5 describes the iterative image recovery algorithm developed using the ideas of convex projections based

restoration. The mathematical theory of POCS is also discussed in Chapter 5. Finally,

Chapter 6 presents conclusions of this study and suggestions for future research.

CHAPTER 2

THE HADAMARD NATURALNESS-PRESERVING TRANSFORM

The Naturalness-Preserving transform (NPT) was first proposed in 1983 by Yarlagadda and Hershey [54]. The NPT is a member of a set of operators known as hybrid transforms. The hybrid transform of an image retains some of the features of the original image. An important feature of a NPT transformed "signal" is that each pixel, point, or segment of the signal contains information about the entire signal. This unique property allows a degraded signal to be reconstructed iteratively from the remaining portion of the transform domain data. The Hadamard NPT (HNPT) has been used for image coding [54], for reconstruction of one-dimensional signals [32], and for reconstruction of missing voice frames [26].

2.1 Naturalness-Preserving Transforms

In general, a hybrid transform can be expressed as a linear combination of orthogonal matrices.

$$\psi(\alpha) = \sum_{i=1}^{l} k_i(\alpha) M_i \qquad (2.1)$$

M_i is an orthogonal matrix and $\sum_{i=1}^{l} k_i(\alpha) = 1$. For the hybrid case of $l = 2$, $\psi(\alpha)$ is

$$\psi(\alpha) = k_1(\alpha)M_1 + k_2(\alpha)M_2 \tag{2.2}$$

where $k_i(\alpha)$ is a weighted function of α. The inverse of $\psi(\alpha)$ is expressed as

$$\psi^{-1}(\alpha) = \frac{1}{k_1^2(\alpha) - k_2^2(\alpha)}[k_1(\alpha)M_1 - k_2(\alpha)M_2] \tag{2.3}$$

and $k_1^2(\alpha) - k_2^2(\alpha) \neq 0$. The transform of a $2^n \times 2^n$ image P is then

$$Q = \psi(\alpha)P\psi(\alpha) \qquad 0 \leq \alpha \leq 1, \ \alpha \neq 0.5 \tag{2.4}$$

The Hadamard NPT and its inverse are defined below with H_n being the normalized Hadamard matrix of order $N = 2^n$.

$$\psi(\alpha) = \alpha I + (1-\alpha)H_n \tag{2.5}$$

$$\psi^{-1}(\alpha) = \frac{1}{2\alpha - 1}[\alpha I - (1-\alpha)H_n] \quad \alpha \neq 0.5 \tag{2.6}$$

H_n is defined by

$$H_n = H_1 \otimes H_{n-1} \tag{2.7}$$

where $\otimes$ denotes the Kronecker product and the lowest order Hadamard matrix, H_1, is

$$H_1 = \frac{1}{\sqrt{2}}\begin{bmatrix} 1 & 1 \\ 1 & -1 \end{bmatrix}. \tag{2.8}$$

For $\alpha = 1$, the transformed image Q is simply the original image. When $\alpha = 0$, Q is the Hadamard transform of the image.

2.2 Image Coding and the HNPT

The two-dimensional NPT of an image is defined by Equation (2.4). Using Equation (2.5) to expand this result for the Hadamard NPT yields

$$\psi(\alpha)P\psi(\alpha) = \alpha^2 P + (1-\alpha)^2 H_n PH_n + \alpha(1-\alpha)[PH_n + H_n P] \tag{2.9}$$

The resulting image is a sum of a weighted version of the original image, a weighted version of the Hadamard transformed image, and a weighted "cross product" image.

Yarlagadda and Hershey proposed the NPT for use in image compression and in reconstruction of degraded images such as jammed or noisy images [54]. Since every transformed pixel contains information about the entire image, missing portions of the received image can be filled in with a known image texture. The iterative algorithm enforces consistency with known values in both the transform domain and the image domain. At the ith iteration, the reconstructed image is given by

$$P_i = \psi(\beta)\hat{Q}_{i-1}\psi(\beta) \quad \text{where} \quad \beta = \alpha/(2\alpha - 1) \tag{2.10}$$

and the transformed image is defined as

$$Q_i = \psi(\alpha)\hat{P}_i\psi(\alpha). \tag{2.11}$$

Regions in the transform domain which are correctly received are not altered during the iterative process. Correct values from Q_0 are retained in each iteration to obtain $\hat{Q}_{i-1}$. In the image domain, a known or constant texture is substituted into the appropriate region of the reconstructed image yielding $\hat{P}_i$. One drawback of this algorithm is the requirement of human intervention to locate the correctly received image data, to define the known texture used in the reconstruction, and to determine the number of iterations required during the reconstruction process.

Data transmission over an asynchronous transfer mode (ATM) network [41] allows for identification of lost packets. The data stream is segmented into fixed-size cells or packets containing the packet header and an information field. The ATM

adaptation layer (AAL) provides the framework for handling transmission errors and packet segmentation and reassembly. By using an appropriate transmission network, image regions that correspond to incorrectly received data can be easily identified by the transmission protocols.

More recently, the HNPT has been successfully used to reconstruct missing frames of voice data. Kohler and Yarlagadda [26] used a reconstruction algorithm similar to the image reconstruction procedure described by Equations (2.10) and (2.11). Coded speech is ordered sequentially in a 2^n x 2^n matrix and transformed using the HNPT. Known background information such as a predetermined background noise or silence can be used to form $\hat{P_i}$. The HNPT reconstruction algorithm performance was compared to frame repetition techniques. Both signal-to-noise comparisons and listening tests demonstrate the effectiveness of the reconstruction procedure. For random packet losses of five to twenty five percent, the HNPT reconstruction algorithm was preferred by listeners over 80% of the time.

Osinubi and King [32] used the one-dimensional HNPT for encoding and restoration of images transmitted over lossy packet networks. A portion of the HNPT coded signal is sent in "guaranteed" packets while the remaining packets are sent if the network traffic is not too heavy. By using the one-dimensional HNPT, a row-scanned image P can be expressed as a vector S and Equation (2.9) is simplified. The transformed signal R is then described by only two weighted components, a weighted version of the original signal and a weighted version of the Hadamard transform of the signal.

$$R = \psi(\alpha)S = \alpha S + (1-\alpha)H_n S \qquad (2.12)$$

For dropped packets, a signal estimate was reconstructed using the available known packets of the HNPT coefficients. Their iterative reconstruction scheme converged for values of $\alpha < 0.5$ and was successful in restoring good quality reconstructions even with 50% packet loss.

2.3 Implementation and Examples

The Hadamard matrix is constructed using the relationship in [53]

$$H_n = \frac{1}{\sqrt{N}} A^n \qquad (2.13)$$

where A is a sparse matrix of order $N = 2^n$ and is defined as

$$A = \begin{bmatrix} 1 & 1 & 0 & 0 & \cdots & & 0 & 0 \\ 0 & 0 & 1 & 1 & \cdots & & 0 & 0 \\ & & & & & \ddots & & \\ 0 & 0 & 0 & 0 & & & 1 & 1 \\ 1 & -1 & 0 & 0 & \cdots & & 0 & 0 \\ 0 & 0 & 1 & -1 & \cdots & & 0 & 0 \\ & & & & & \ddots & & \\ 0 & 0 & 0 & 0 & & & 1 & -1 \end{bmatrix}. \qquad (2.14)$$

Using Equations (2.9) and (2.13), the HNPT of an image can be constructed using only additions and subtractions. Each multiplication by matrix A requires $N^2/2$ additions and $N^2/2$ subtractions. Omitting scaling constants, Equation (2.9) can be computed using $(4\log_2 N + 3)N^2$ addition operations. Fast algorithms similar to the FFT algorithm have been developed to compute the Hadamard transform [44] [53].

Figure 2.1 shows the original 512 x 512 *Zelda* image, the transformed images for two values of alpha, and the corresponding coefficient histograms. As expected, larger values of α allow the original image to be evident in the image of the HNPT coefficients
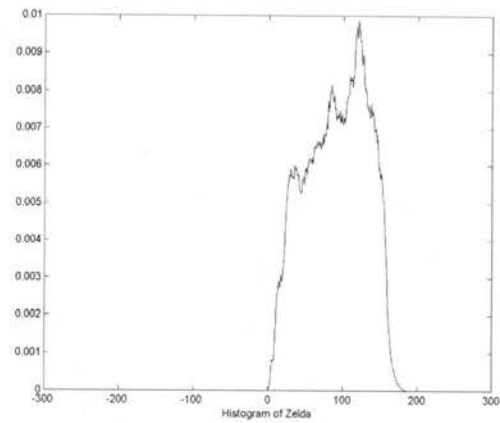
a) Original *Zelda* and histogram
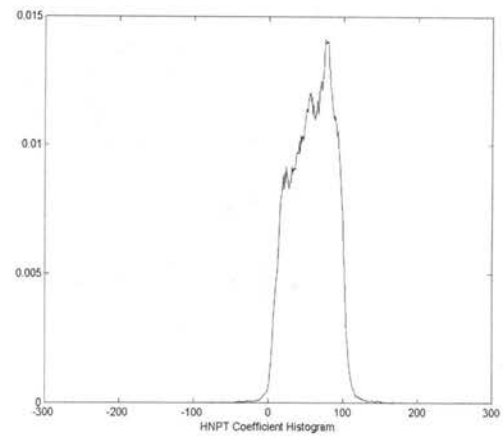
b) HNPT coefficient image and coefficient histogram, $\alpha = 0.8$
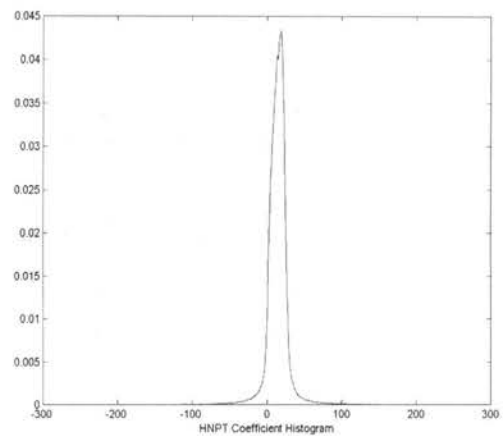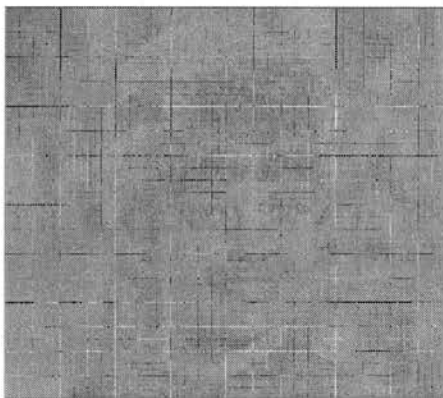
c) HNPT coefficient image and coefficient histogram, $\alpha = 0.4$

Figure 2.1 *Zelda* and HNPT Coefficient Histograms

and the transform coefficient histograms to have the same general shape as the original image. As α decreases, the percentage of transform coefficients surrounding the coefficient mean increases dramatically and the histogram becomes more peaked. The shape of the HNPT coefficient histogram is indicative of the probability density function (pdf) characteristics that best model the data.

2.4 Statistical Properties of HNPT Coded Images

This section presents a brief look at the statistical properties of HNPT coefficients including calculation of the mean, variance, and correlation coefficients for a variety of test images. The horizontal and vertical correlation coefficients are calculated for non-sequency ordered HNPT data with further discussion of the shape of the coefficient distribution reserved for Chapter 4. A sample of the results for the test image *Goldhill* is presented in Table 2.1 for selected values of α. The statistics of the other test images follow the same general characteristics.

For values of $\alpha < 0.2$, the mean is significantly smaller than the standard deviation and is relatively close to zero. As expected, the correlation coefficients are small for values of $\alpha < 0.5$. Decorrelation of the image data and the ability of a transform to pack the signal energy into a small number of transform coefficients are desired qualities for compression purposes. For this reason, only values of $\alpha < 0.5$ will be used to encode the image data. Looking at values of $\alpha < 0.2$ reveals that over 90 percent of the coefficient energy is contained in an 8 x 8 block of the lowest sequency coefficients. In the following chapters, $\alpha = 0.2$ will be the HNPT weighting coefficient used for most examples.

TABLE 2.1 Statistics of HNPT Coefficients of Goldhill

α	Mean	Standard Deviation	Correlation ρ_h	Coefficients ρ_v
0.00	0.89	122.47	0.005	0.001
0.10	3.64	102.56	0.038	0.016
0.20	8.26	86.78	0.098	0.060
0.30	14.73	74.70	0.183	0.135
0.40	23.07	65.57	0.283	0.236
0.49	31.08	59.79	0.363	0.326
0.60	45.33	52.69	0.478	0.467
0.70	59.26	47.80	0.580	0.597
0.80	75.05	44.35	0.709	0.746
0.90	92.70	44.02	0.853	0.887
1.00	112.21	49.07	0.937	0.941

2.5 Summary

This chapter provides an introduction to the Hadamard Naturalness-Preserving Transform and its application to image coding. Previous research using the HNPT for both image and speech reconstruction is presented. The effects of transforming an image using the HNPT are demonstrated and the general statistical properties of HNPT coded images are summarized for a range of weighting constants. Chapter 3 provides additional introductory material in the areas of image coding and image reconstruction techniques.

CHAPTER 3

INTRODUCTION TO IMAGE COMPRESSION AND RESTORATION

Compression techniques can be classified as either lossless or lossy. Lossless

compression algorithms preserve all the image information while achieving only modest

compression ratios. The need for higher compression ratios for image storage and image

transmission requires a reduction in the amount of data used to represent an image. This

loss of information leads to degradation of image quality and the need for image

restoration algorithms. Image coders consist of three basic stages. Figure 3.1 shows the

basic block diagram for a transform based image coder [46].

```
Original   →  Signal        →  Quantization  →  Lossless     →  Compressed  →
Image         Decomposition\                     Entropy         Bitstream
              Transform                           Coding
```
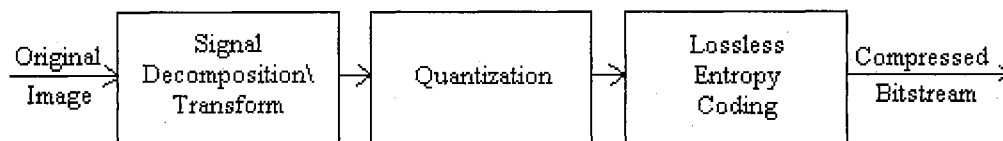
Figure 3.1 Generic Image Coder

The first stage is a lossless process which decorrelates the data either through

subband coding or transform coding. Most of the loss occurs in the second stage where

the data is quantized using either scalar, vector, or predictive quantization methods. The

quantization process leads to a trade-off between minimizing the number of bits or

maintaining acceptable image quality. For subband coders, zigzag scanning and run-

length coding can also be used to increase compression ratios. The final coding stage, entropy coding, is a reversible lossless step.

At high compression ratios, the transform/subband coefficients are coarsely approximated. As a result of the quantization process, the decoded image contains distortions. One method of reducing the number of artifacts in the decoded images is to apply some kind of image post-processing. Also, perfect transmission of the compressed image data over a communications channel is not guaranteed due to noise and/or jamming. The loss of any encoded data introduces additional artifacts in the reconstructed image. The technique of projections onto convex sets (POCS) is one method of removing image artifacts caused either by compression or by channel loss.

This chapter reviews both transform and subband based coders. Included are examples of baseline JPEG compression and subband compression. The differences in compression artifacts between the two algorithms are noted. Also included is a general discussion of image restoration problems and specific examples of POCS based restoration schemes. For a more complete discussion of image coding techniques, the reader is referred to the following texts ([22], [36], and [46]). This chapter concludes with an introduction to packet-based networks, specifically asynchronous transfer mode (ATM) networks. Properties of ATM networks that are relevant to the reconstruction process are listed.

3.1 Block-Based Transform Coding

Image transformation can be looked at as a decomposition of the data into its frequency or spectral components. Theoretically, the Karhunen-Loeve transform (KLT)

is optimal in terms of coefficient decorrelation and energy compaction [2]. The KLT achieves exact diagonalization of the image's autocovariance matrix. This results in most of the image energy being concentrated in a small fraction of the transform coefficients. Since the KLT is image dependent and computationally complex, the discrete cosine transform (DCT) provides a fast, efficient method of achieving close to exact diagonalization of the autocovariance matrix.

3.1.1 The Discrete Cosine Transform

The discrete cosine transform matrix is a separable, unitary transform matrix. The forward transform of an N x N image block P is obtained by applying the transform matrix D first to the columns

$$Q' = DP \tag{3.1}$$

and then applying the transform to the resulting rows of Q'.

$$Q = Q'D^T = DPD^T \tag{3.2}$$

where D^T denotes the transpose of D and Q is the N x N matrix of transform coefficients. The transform matrix D contains the N orthonormal discrete cosine basis vectors written as its rows.

$$D_{k,m} = \alpha_m \cos\left[\frac{(2m+1)k\pi}{2N}\right]$$
$$where \quad \alpha_m = \sqrt{\tfrac{1}{N}} \quad k = 0 \tag{3.3}$$
$$= \sqrt{\tfrac{2}{N}} \quad k = 1, 2, ..., N-1$$

$Q_{o,o}$ is the DC or low frequency coefficient and corresponds to the average intensity level in the image block. The remaining coefficients are referred to as AC coefficients. The

inverse transform provides a mapping from the transform domain coefficients Q back to image space.

$$P = D^T Q D \qquad (3.4)$$

The matrix transform can also be expressed in vector space form. Let p denote the vector representation of the image matrix P. p is a N^2 x 1 vector obtained by lexicographically ordering P by either its rows or columns. Similarly let q denote the vector representation of the transform coefficients. Then the two dimensional unitary transform and its inverse written in vector form are given by

$$q = D p \qquad \text{and} \qquad p = D^T q . \qquad (3.5)$$

3.1.2 JPEG

At the present time, block-based transform coders (specifically JPEG) are the most familiar coders to the average computer user [35]. The JPEG still image standard includes four modes of compression: sequential, lossless, progressive, and hierarchical. The sequential, baseline JPEG algorithm segments the image data into 8 x 8 pixel blocks and each image block is encoded in a left-to-right, top-to-bottom scan. The discrete cosine transform is used to decorrelate the data. The transform coefficients are quantized and data is further compressed using entropy encoding. As an additional step after quantization, the DC coefficients are encoded using a first order predictor and lossless differential encoding while the AC coefficients are scanned in a zigzag order to create a one dimensional sequence amenable to run-length encoding. Figure 3.2 illustrates the basic JPEG encoding procedure. Decoding follows the encoding process in reverse order.
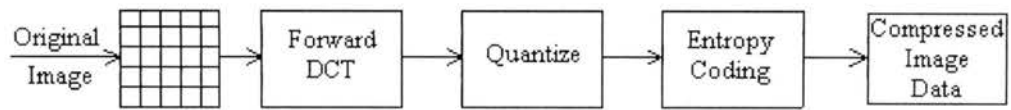
Figure 3.2 Baseline JPEG

(a)
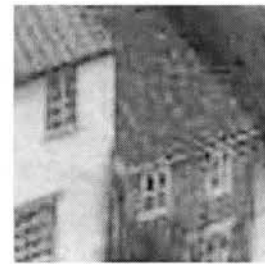
(b)

(c)

(d)

Figure 3.3 Example of Transform Coded *Goldhill* Using Baseline JPEG
(a) Compression Ratio 7.96:1   (b) Selected subregion
(c) Compression Ratio 20.43:1(d) Selected subregion

Figure 3.3 provides a representative example of JPEG compression performance at approximate compression ratios of 8:1 and 20:1. The PSNR is 30.28dB and 26.63dB respectively for Figures 3.3a and 3.3c. These images were obtained from The Waterloo BragZone and Fractals Repository website. The site is maintained by the University of Waterloo, Ontario and provides an excellent resource in comparing the results from different image compression algorithms. The most noticeable artifact in JPEG compressed images is "blocking" which is due to the structure of the algorithm. By processing pixel blocks independently, the correlation between blocks is removed and artificial boundaries are introduced in the reconstructed image. Some "ringing artifacts" are also evident near edges as a result of quantizing and eliminating some high frequency coefficients.

3.2 Subband Coding

Subband coding involves filtering an image to create subimages that represent smaller frequency bands than the original image's frequency band. Each subband tends to have features similar to the original image content. Block transform coding also provides frequency band information when the transform coefficients are arranged differently. By reordering the block transform coefficients, the newly formed blocks (subbands) correspond to regions with different frequency components [4][22]. Conversely, subband coefficients can be reordered to provide spatial information [49]. In Figure 3.4, the 2 x 2 blocks of transform coefficients are rearranged to form their corresponding subbands.

a b	a b
c d	c d
a b	a b
c d	c d

a a	b b
a a	b b
c c	d d
c c	d d

(a)   (b)
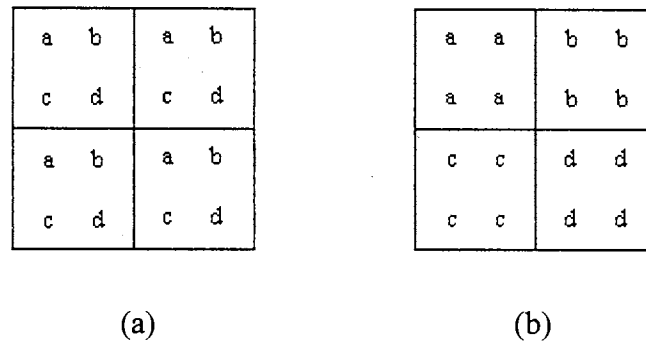
Figure 3.4 Relationship Between Block Transform Coding and Subband Coding
Output Coefficients (a) Block transform coding output (b) Subband coding output

Subband coding divides a signal into frequency bands. The subband

representation is obtained by repeated convolutions with a pair of FIR filters in both the

horizontal and vertical directions. After subsampling by two the process is repeated

either on the lowpass subband (octave decomposition) or on each subband (full-band

decomposition). This process is generally referred to as subband analysis. The decoder

performs the inverse of the operation described above. The subband signals are fed into

the synthesis filter bank where they are upsampled, filtered, and summed. Figure 3.5

depicts a one-dimensional two-band filter bank system. For subband image coding, the

analysis/synthesis process occurs in both the horizontal and vertical directions. For full-

band decomposition, each subband is fed into the analysis filter bank. As a result, there

will be 4^j subbands where j is the number of decomposition levels. Octave

decomposition results in $4 + 3(j - 1)$ subbands. In this case, only the lowpass subband is

passed to the filter bank.
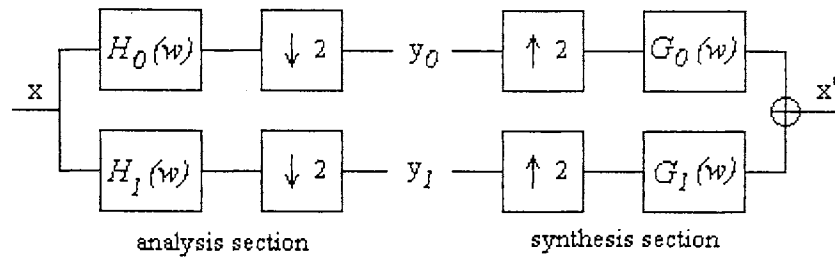
Figure 3.5 Two-band Analysis/Synthesis Filter Bank

Several techniques are available for quantizing the subband coefficients. One option is to independently quantize each subband. High frequency subbands have been quantized using both Lloyd-Max quantizers [48] or uniform threshold quantizers [45]. The lowpass subband is a lowpass filtered subsampled version of the original image and can be encoded using JPEG [45] or DPCM [50]. Vector quantization across the bands is another quantization option [47] and is easiest when the subbands are the same size as in full-band decomposition.

Figure 3.6 shows two examples of subband coding from the University of Waterloo database. The coder used is the Efficient Pyramidal Image Coder (EPIC) developed by Simoncelli and Adelson at MIT Media Labs [1] [40]. EPIC uses a biorthogonal wavelet decomposition combined with run-length and Huffman entropy encoding. For compression ratios of approximately 8:1 and 20:1, the PSNR is 29.93dB and 26.45dB respectively for Figures 3.6a and 3.6b. A good example of ringing noise can be seen in the roof lines and other house edges. At higher compression ratios, JPEG suffers from blockiness while the subband encoded images appear blurry.

(a)

(b)

(c)

(d)
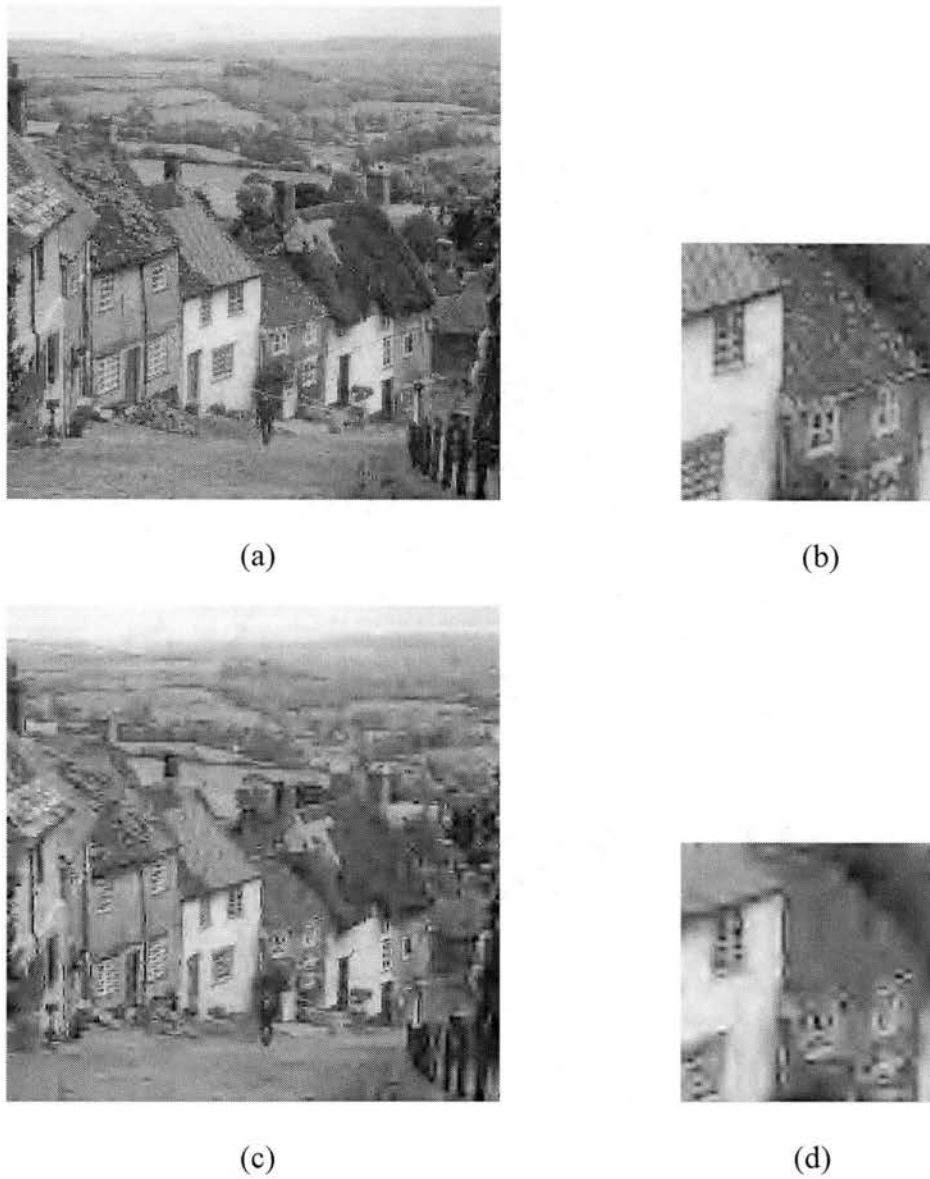
Figure 3.6 Example of Subband Coded *Goldhill* Using Wavelet Based EPIC Coder
(a) Compression Ratio 8.47:1   (b) Selected subregion
(c) Compression Ratio 20.31:1 (d) Selected subregion

3.2.1 Subband Filters

The relationship between the input and the output of the analysis/synthesis system shown in Figure 3.5 is given by

$$X'\left(e^{jw}\right) = \tfrac{1}{2}X\left(e^{jw}\right)\left[H_0\left(e^{jw}\right)G_0\left(e^{jw}\right) + H_1\left(e^{jw}\right)G_1\left(e^{jw}\right)\right]$$
$$+ \tfrac{1}{2}X\left(e^{j(w+\pi)}\right)\left[H_0\left(e^{j(w+\pi)}\right)G_0\left(e^{jw}\right) + H_1\left(e^{j(w+\pi)}\right)G_1\left(e^{jw}\right)\right] \qquad (3.6)$$

where $H_0\left(e^{jw}\right)$ and $H_1\left(e^{jw}\right)$ are the lowpass and highpass analysis filters and $G_0\left(e^{jw}\right)$ and $G_1\left(e^{jw}\right)$ are the lowpass and highpass synthesis filters. The second term in Equation (3.6) is the aliasing term. Perfect reconstruction filters, $X'\left(e^{jw}\right) = X\left(e^{jw}\right)$, eliminate the aliasing component.

A quadrature mirror filter (QMF) analysis/synthesis system is one of the most commonly used for subband decomposition. QMF's provide near-perfect reconstruction and are derived from a single lowpass filter, H_o [7]. The highpass filters are formed simply by modulating the lowpass filter. The filters are symmetric and are defined by

$$G_0\left(e^{jw}\right) = H_o\left(e^{jw}\right)$$
$$H_1\left(e^{jw}\right) = H_o\left(e^{j(w+\pi)}\right) . \qquad (3.7)$$
$$G_1\left(e^{jw}\right) = -G_o\left(e^{j(w+\pi)}\right)$$

An excellent overview of subband coding using QMF's is given in [36] and [8].

3.2.2 Hadamard Subband Coding

Yu and Mitra [58] have formalized a method for subband coding with the Hadamard transform. One advantage of Hadamard transform coding is the simplicity of the operation. Only additions and subtractions are required to perform the Hadamard transform.

Consider an N x N image P. If the image is divided into subimages of size M x M, there are L^2 subimages where $L=N/M$ and is assumed to be an integer. Each subimage

contains spatial information about a specific region. To obtain frequency information, the spatial blocks must be transformed into M^2 *(L* x *L)* subbands.

P can be described as an ordered grouping of the *M* x *M* spatial subimages. For the case of *M* = 2, $B_{i,j}$ will be a 2 x 2 pixel block.

$$P = \left(B_{i,j} \right) \qquad i,j = 1,2,\dots,L \tag{3.8}$$

$$B_{i,j} = \begin{bmatrix} b_{1,1} & b_{1,2} \\ b_{2,1} & b_{2,2} \end{bmatrix} \tag{3.9}$$

Rewriting $B_{i,j}$ as vector $b_{i,j}$ the pixel block can be transformed by a M^2 x M^2 matrix *D*.

$$b_{i,j} = \begin{bmatrix} b_{1,1} & b_{1,2} & b_{2,1} & b_{2,2} \end{bmatrix}^T \tag{3.10}$$

The result of this operation can be written as

$$c_{i,j} = D b_{i,j} \tag{3.11}$$

Just as $B_{i,j}$ was reordered, the vector $c_{i,j}$ can be reordered to form the matrix $C_{i,j}$.

Lowpass filtering of $B_{i,j}$ is equivalent to

$$\tfrac{1}{4}\left(b_{1,1} + b_{1,2} + b_{2,1} + b_{2,2} \right). \tag{3.12}$$

The row gradient is given by

$$\tfrac{1}{4}\left(b_{1,1} + b_{1,2} - b_{2,1} - b_{2,2} \right) \tag{3.13}$$

and the column gradient is given by

$$\tfrac{1}{4}\left(b_{1,1} - b_{1,2} + b_{2,1} - b_{2,2} \right). \tag{3.14}$$

Finally, diagonal edge information is obtained from

$$\tfrac{1}{4}\left(b_{1,1} - b_{1,2} - b_{2,1} + b_{2,2} \right). \tag{3.15}$$

Combining Equations (3.12) – (3.15), the transformation matrix *D* is given by a scaled version of the Hadamard transform.

$$D = \frac{1}{4} \begin{bmatrix} 1 & 1 & 1 & 1 \\ 1 & -1 & 1 & -1 \\ 1 & 1 & -1 & -1 \\ 1 & -1 & -1 & 1 \end{bmatrix}$$

(3.16)

The lowpass subband can be passed on to the same set of filters to provide multi-resolutional information. Figure 3.7 shows the results of Hadamard subband coding on *Lena*.

Figure 3.7 Hadamard Subband Coding of *Lena*

3.3 General Image Restoration

The classical image restoration problem assumes two dominant types of degradation – blurring and noise. The degradation model is defined by

$$\hat{y} = H x + n \qquad (3.17)$$

where $\hat{y}$ is the observed image, x is the ideal or original image, H is the blurring operator, n models the noise, and $\hat{y}$, x, and n are lexicographically ordered vector representations of their respective images. Blur can be caused by motion between the camera and the scene or it can be caused by the imaging system being out of focus. The noise is generally modeled as an additive white Gaussian noise process.

The goal of the restoration process is to operate on the corrupted image to restore an estimate that closely approximates the original image. Generally some knowledge of the blurring function, the noise, and the original image are assumed. By assuming a model for the point spread function of the imaging system (blur model), the problem becomes one of inverting Equation (3.17). Since inverse filtering techniques lead to an increase in noise effects, constrained restoration (iterative algorithms) offer a trade-off between noise smoothing and maintaining image sharpness. The most common restoration filter, the Wiener filter, and the Kalman filter both fall into the non-iterative category.

Given an estimate of the point spread function, the Wiener filter is optimized to obtain the minimum mean square error. The filter's transfer function [17] is given by

$$\frac{H^*(u,v)S_x(u,v)}{|H(u,v)|^2 S_x(u,v) + S_n(u,v)} \qquad (3.18)$$

where $H(u,v)$ is the blur transfer function, $S_x(u,v)$ is the image spectral density, and $S_n(u,v)$ is the noise spectral density. In reality, estimation of $S_x(u,v)$ and $S_n(u,v)$ is the main difficulty in implementing the Wiener filter. Constrained least squares restoration

requires an estimate only of the noise mean and variance not the spectral density. The solution is given by

$$\hat{x} = [H^T H + \gamma C^T C] H^T \hat{y} \qquad (3.19)$$

where C is a smoothness operator and γ is a constraint constant. Other iterative, regularized restoration methods are available [24] [25].

The projection approach to image restoration chooses constraints based on prior knowledge about image characteristics. The difference between set-theoretic methods and regularized restoration is that the convex set solution is any image that satisfies the defined constraints. The more restrictive the constraint sets, the narrower the possible solution space. One drawback to convex set restoration is the computational expense incurred. Several iterations are usually required before convergence. These methods are only suitable for image decoders with computational power available.

3.4 Image Restoration Algorithms Incorporating POCS

This section reviews the recent image restoration literature where POCS based algorithms have been implemented to improve the quality of compressed images. Convex projection techniques have been used to improve JPEG encoded images, to improve video sequences, and to enhance primitive-based wavelet coding.

3.4.1 Reduction of Blocking Artifacts in Still Images

The use of a block DCT compression algorithm automatically introduces artificial boundaries in the reconstructed image at high compression ratios. Rosenholtz and Zakhor proposed the use of two projection operators to reduce these blocking artifacts in JPEG

coded images [39]. The first projection operator uses the set of band-limited images with a specific cut-off frequency. By applying an ideal lowpass filter to the received image, this constraint is meant to reduce both the horizontal and the vertical blocking artifacts that are present. The second projection operator restricts the decoded DCT coefficients to their proper quantization intervals. Any DCT coefficient that lies outside its quantization range is projected to the appropriate range boundary. The projection for the quantization constraint is defined as

$$P_{Limit} f(x,y) = \begin{cases} a & f(x,y) < a \\ f(x,y) & a \le f(x,y) \le b \\ b & f(x,y) > b \end{cases} \qquad (3.20)$$

where a and b are the quantization interval boundaries. Equation (3.20) can also be used to ensure valid pixel intensities ($[a,b] = [0,255]$). Rosenholtz and Zakhor assumed that an ideal low-pass filter was the filter used in the band-limiting projection operation. However, the filter specified in [39] is not an ideal low-pass filter and thus the filtering constraint set is not convex. Their algorithm instead solves a constrained minimization problem. The quantization constraint is defined by a convex set while the lowpass filtering minimizes the blocking artifacts.

Care must be taken to properly choose constraint sets and to correctly define projection operators. (Note: $P_{Limit} f(x,y)$ detailed above is a valid projection operator [56]) Improper constraints result in either an empty intersection or a solution which is actually based on a different methodology than anticipated.

Yang, et al [51] also proposed convex constraints based on knowledge of the DCT coefficient characteristics and on image smoothness. The quantization constraint insures consistency with the encoded data by enforcing quantization interval boundaries. The

smoothness constraint is based on the characteristics of the original image and focuses specifically on smoothness between block boundaries. This constraint is defined by limiting the variation of the pixel values between the boundaries of adjacent blocks. Yang's algorithm reduced blocking artifacts and improved the signal-to-noise ratio of the recovered image in fewer than 20 iterations.

3.4.2 Edge Preservation

By nature, compression algorithms truncate high frequency coefficients. Zeroing these coefficients causes Gibbs artifacts [30], i.e. ringing near image edges. The sharpness of the edges is an important factor in the perceived quality of a compressed image. Su and Mersereau [42] combine edge preservation with a quantization constraint and lowpass filtering for post-processing of JPEG compressed images. Edges are preserved during each iteration by limiting the difference between the original decompressed image and the restored image at each pixel location. To enhance the edge-preserving constraint, individual pixels are classified as uniform, texture, or edge pixels and each block is labeled by the strength of its edges.

The smoothing of the output image is not part of the convex projections process. By combining the lowpass filtering with the convex constraints and wisely choosing the filter coefficients, the iterative algorithm becomes a constrained optimization problem. The algorithm presented is simple and effective. Both ringing and blocking artifacts are reduced in fewer than five iterations. Su and Mersereau also present additional comparisons between their algorithm and Zahkor's algorithm mentioned earlier in

Chapter 3.4.1. Su and Mersereau's restoration scheme offers less blurring, sharper edges, and a slightly increased signal-to-noise ratio.

The optimal reconstruction procedure developed by Zhong [60] incorporates convex constraint sets in a constrained optimization algorithm. The quantization constraint defined by Equation (3.20) is combined with an "evolution procedure" to reduce ringing artifacts. The evolution procedure is designed to reduce blocking artifacts by decreasing the total variations and to reduce Gibbs artifacts by updating high frequency coefficients associated with edges. Further discussion of Zhong's evolution procedure is given in [59]. The evolution process removes compression artifacts while the projections operator keeps transform coefficients in their appropriate quantization range. The optimal reconstruction technique described in [60] was applied to JPEG encoded images with a compression ratio of 17:1. The algorithm successfully reduced blocking artifacts without blurring the image and improved the appearance of ringing artifacts.

3.4.3 Reduction of Blocking Artifacts in Video

Coded video sequences can also suffer from blocking artifacts. Additional errors due to transmission losses further affect the quality of the received video sequence. Sun and Kwok [43] proposed a restoration algorithm based on the characteristics of the good blocks that are surrounding blocks lost in transmission. An important contribution of this algorithm is the inclusion of edge continuity information. Additional constraints require restored pixels to lie in a valid intensity range and impose smoothness.

P$_{Limit}$ defined in Equation (3.20) can be used to impose the constraint of valid pixel values. The edge and smoothness constraints are defined in the Fourier domain by a similar convex set description – the transform coefficients of the data are required to lie in a prescribed region. P$_{smooth}$ is a lowpass filter that zeroes Fourier coefficients outside a cutoff frequency R_{th}. F is the N x N DFT and m and n are the Fourier domain indices.

$$P_{smooth}f(x,y) = \begin{cases} 0 & \sqrt{m^2 + n^2} > R_{th} \\ F(m,n) & otherwise \end{cases} \qquad (3.21)$$

In the Fourier domain, edge coefficients lie in a direction that is orthogonal to the edge. Thus, P$_{edge}$ is a directional bandpass filter with bandwidth B_{th}. Edges are assigned a direction based on the gradient angle θ. The allowed edge categories lie in one of eight regions equally spaced from θ=0° to θ=180°.

$$P_{edge}f(x,y) = \begin{cases} 0 & \left| m - n * \tan(\theta + 90°) \right| > B_{th} \\ F(m,n) & otherwise \end{cases} \qquad (3.22)$$

The algorithm begins by identifying lost blocks and determining if a block is smooth or contains edges. Using the projection operators listed above, a damaged block and its eight neighboring blocks are first combined into a larger block. This larger block is identified as either a smooth block or an edge block before applying the projection operators. The definition of P$_{Limit}$ is expanded so that the pixel values in neighboring good blocks remain the same and only the pixel values in the damaged block are altered. The projection operator P$_C$ ensures that correctly received values are not altered by the restoration process and is described by

$$P_C f(x,y) = \begin{cases} k(x,y) & M(x,y) = 0 \\ f(x,y) & M(x,y) = 1 \end{cases} \qquad (3.23)$$

where $M(x,y)$ denotes the location of the correctly received pixel values $k(x,y)$. Although P_{Limit} and P_C were combined into one operator in this paper, they can also be applied independently.

For the still image tests, good quality restored images were obtained in less than ten iterations. Applying the POCS algorithm to video sequences yielded better performance than motion compensated block copying. The best results were obtained when restoring mid frequency and low frequency blocks.

3.4.4 Applications to Subband/Wavelet Compressed Images

Croft and Robinson [6] used a wavelet decomposition to approximate a multiresolution Difference-of-Gaussians (D-o-G) filter and to perform compression using the second derivative extrema of the D-o-G filter. In the high frequency subbands, the largest magnitude watershed and watercourse lines are calculated and chain-coded. Watershed and watercourse lines describe the ridges and valleys of the image surface. The large amplitude extrema identify the most significant edge information. The lowpass subband is compressed by subsampling followed by DPCM coding.

The projection operators used in the recovery/decoding process are the discrete wavelet transform and P_C. For this algorithm, P_C is used to impose consistency with the encoded data in each subband. First, the values of the lowpass wavelet coefficients are preserved during each iteration. The smoothing characteristics of the lowpass wavelet filter also help prevent the creation of any false extrema in the high frequency subbands. Edge information is kept consistent by updating the highpass coefficients only at watershed and watercourse locations.

Using a subband coder and POCS, Croft and Robinson developed an iterative reconstruction scheme that provides better quality reconstructed images than a JPEG coder. Improvements were most noticeable in edge continuity. However for highly textured, finely detailed images such as *Goldhill*, JPEG provides better compression results.

3.5 Image Transmission over Asynchronous Transfer Mode Networks

Transmission of data over a communications channel frequently results in the loss or corruption of the original data. Data loss can be due to noise, network congestion, signal degradation, jamming, etc. The loss of image data presents a reconstruction problem at the decoder. This section provides an introduction to asynchronous transfer mode (ATM) networks and details some of the packetization requirements for successful reconstruction of lost image data [41].

3.5.1 ATM Networks

ATM networks transmit data in fixed-size cells or packets. The use of fixed-size cells allows the switching mechanism to be implemented in hardware so that packets are switched more efficiently. The data's route between switches or nodes is determined prior to transmission over a virtual circuit. By establishing a predetermined path, routing decisions are not required at each node. One disadvantage to this approach is that packets cannot be routed away from congestion. The buffering, queuing, and error control necessary at each node can incur additional delay. In the datagram approach, each packet is treated as a separate unit. By treating packets individually, the packets can be routed

around any congestion or node failure that develops in the network. This thesis considers use of the virtual circuit approach. Packets are transmitted in a known order and the sequencing information is known at the receiver.

ATM packets consist of a 5 byte header and 48 byte data field. The header contains information necessary for routing and prioritization of packets. The ATM adaptation layer (AAL) provides the framework for handling of transmission errors and packet segmentation and reassembly for different types of data. Addition of information such as sequence numbers and error correction codes adds some overhead and decreases the available payload. The additional header information within the packet payload allows for identification of lost packets and bit error correction within a packet which is essential for image transmission.

3.5.2 Transmission Assumptions for Image Reconstruction

The packet-based transmission network described above has several properties that are necessary for reconstruction of lost image data. The ATM adaptation layer provides for error correction within a packet and insertion of sequence numbers. Other assumptions about packetization of HNPT coded image data for facilitating image reconstruction at the decoder include segmenting and interleaving the coefficient data.

Segmentation of the data can occur in either the spatial or the frequency domain. For spatially based packetization, bursty errors in the network can cause loss in adjoining areas of the image. Interleaving the data before packetization avoids the problem of large areas of loss. Compression techniques such as quantization, run-length encoding and Huffman encoding are allowable as long as codewords fit within the packet payload.

Arithmetic coding among several packets is not allowable. In this case, loss of a packet causes loss of synchronization at the decoder [18].

3.6 Summary

Both DCT based encoders and subband encoders provide fast, efficient algorithms for compressing image data. The artifacts incurred at low bit rates for either compression technique and possible loss of data during transmission suggest the option of additional post-processing at the decoder.

Current research employs POCS techniques within a constrained minimization algorithm to improve the quality of compressed images. These image restoration techniques focus on the decoding phase of an image coder and allow the incorporation of *a priori* knowledge in the decoding process. Convex constraints based on image smoothness, allowable pixel magnitudes, allowable pixel variations, and consistency with the decoded data have been used successfully. It is important to note that POCS based restoration techniques are applied in the post-processing phase of an image coder. Since several iterations are usually required for convergence of the algorithm, there is a computational cost along with delays associated with these methods. Using these examples, constraints can be developed which describe the characteristics of a HNPT encoded signal.

CHAPTER 4

QUANTIZATION AND CODING OF HNPT COEFFICIENTS

To design an effective quantizer, the shape of the coefficient density function distributions should be modeled accurately. For discrete cosine transform coding, Reininger and Gibson [38] determined that non-dc coefficients were better modeled as a Laplacian distribution than as a Gaussian or Rayleigh distribution. For subband coding, the generalized Gaussian probability density function provides a better fit to the subband data than the Laplacian density function [45] [48]. Another popular quantization option used in subband coding is uniform threshold quantizers [9]. These uniform quantizers perform almost as well as optimally designed entropy constrained quantizers.

4.1   Histogram Fitting

For large values of α ($0 \leq \alpha \leq 1$, $\alpha \neq 0.5$), i.e. $\alpha > 0.7$, the HNPT histogram exhibits the characteristics of the original image histogram. As the value of α decreases, the histogram exhibits more of the Hadamard characteristics and becomes more peaked and narrow as seen in Figure 2.1c. The generalized Gaussian probability density function was considered as a possible model for the HNPT coefficient histogram. The generalized Gaussian pdf is given by

$$p(x) = a \exp\left\{-|bx|^{\gamma}\right\} \tag{4.1}$$

where a and b are defined as

$$a = \frac{b\gamma}{2\Gamma\left(\frac{1}{\gamma}\right)} \quad \text{and} \quad b = \frac{1}{\sigma_x}\sqrt{\frac{\Gamma\left(\frac{3}{\gamma}\right)}{\Gamma\left(\frac{1}{\gamma}\right)}}. \tag{4.2}$$

In Equation (4.2), $\Gamma(\ )$ is the Gamma function and γ is a shape parameter which describes the exponential decay. For $\gamma = 1.0$, Equation (4.1) becomes the Laplacian pdf and $\gamma = 2.0$ results in the Gaussian pdf. However, for Hadamard coefficients, a gamma density function defined by

$$p(x) = \frac{b^{\gamma}}{2\Gamma(\gamma)}e^{-b|x|}|x|^{\gamma-1} \quad \text{and} \quad b = \frac{(\gamma^2 + \gamma)^{1/2}}{\sigma_x} \tag{4.3}$$

provides a good fit with the data [10] [14]. For the gamma pdf a shape parameter $\gamma = 1.0$ also results in the Laplacian. Figure 4.1 compares the HNPT ($\alpha = 0.2$) histogram with the gamma pdf and the generalized gaussian pdf. For appropriately chosen values of γ, the overall shape of the density functions are very similar. In the figure below, there are minor differences in peak height and in the pdf's shape at the tails. As $|x| \to \infty$, both the generalized gaussian and the gamma pdf have a broader tail than the HNPT histogram.
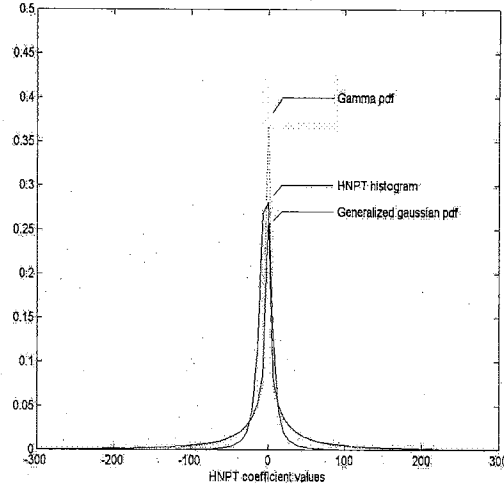
Figure 4.1 Probability Density Functions (a) Gamma pdf
(b) HNPT histogram (c) Generalized Gaussian pdf

4.2 Determination of HNPT Histogram Characteristics

The Kolmogorov-Smirnov (KS) test was used to determine goodness-of-fit between the histogram data and the two density functions described above for values of $\alpha < 0.5$. The KS test statistic, $t_{KS,}$ provides a distance measure between the sample data's distribution function $F_x(\ )$ and a given distribution function $F(\ )$. The density function which minimizes the KS distance measure is considered to provide the best fit with the data. The KS test statistic is defined by

$$t_{KS} = \sqrt{M} \mathop{\max}_{i=1,2,\ldots,M} \left| F_x(x_i) - F(x_i) \right|. \tag{4.4}$$

The KS test was performed on the zero mean HNPT coefficient distribution of ten, 8 bit monochrome images. The image data set consists of seven images of size 256 x 256 pixels and three images of size 512 x 512 pixels. The HNPT weighting constant, α, was incremented over the range $0 \le \alpha < 0.5$. The range of γ for the generalized gaussian was

$0.02 \leq \gamma \leq 1.0$ while allowable values for the gamma distribution shape parameter were $0.05 \leq \gamma \leq 1.0$. The best value of γ minimizes the Kolmogorov-Smirnov distance measure for a given distribution function. For selected values of α, Table 4.2 lists the best values of γ for both density functions.

The results can be summarized as follows. For $\alpha = 0$, a Hadamard transformed image, our best fit γ differs slightly from the values presented in [14]. Our tests indicate that $\gamma = 0.43$ provides a better fit over the image set used rather than $\gamma = 0.5$. Also, the shape parameter values listed for the gamma density function differ from the results presented in [10]. With $\gamma = 3.0$, the gamma density function provides a good fit at the tails of the variance normalized HNPT coefficient data, however, it does not provide an accurate description of the coefficient behavior close to zero [11].

Using the shape parameter values listed in Table 4.1, both the generalized gaussian and the gamma density functions provide a good fit with the high sequency HNPT data. The results are close enough that either density function can be selected for an appropriately chosen value of γ. Table 4.2 summarizes the average values of γ for both density functions. For $0 \leq \alpha < 0.5$, the value of γ varies more when using the generalized gaussian pdf to model the transform data. In order to simplify the quantizer design, the gamma density function will be used with either $\gamma = 0.5$ or $\gamma = 0.6$.

The KS test was also performed on a selected portion of the low sequency HNPT coefficients. Sequency is a generalization of the concept of frequency and is defined as one half of the number of zero-crossings per unit time [2]. Sequency can be used to describe functions whose zero-crossings are not equally spaced over an interval.

Table 4.1 Best Value of γ Determined by Kolmogorov-Smirnov Test

Image	α	Best Value of γ for Generalized Gaussian density function						Best Value of γ for Gamma density function					
		0.00	0.10	0.20	0.30	0.40	0.49	0.00	0.10	0.20	0.30	0.40	0.49
Bird		0.19	0.19	0.26	0.36	0.39	0.33	0.36	0.47	0.60	0.69	0.55	0.53
Bridge		0.26	0.26	0.30	0.36	0.37	0.42	0.50	0.54	0.67	0.60	0.65	0.72
Cameraman		0.26	0.26	0.29	0.34	0.36	0.36	0.51	0.53	0.67	0.60	0.65	0.72
Goldhill		0.25	0.25	0.29	0.35	0.41	0.49	0.48	0.54	0.57	0.65	0.68	0.73
Lena		0.22	0.22	0.26	0.32	0.34	0.37	0.43	0.50	0.57	0.57	0.59	0.63
C256		0.17	0.31	0.34	0.25	0.37	0.43	0.25	0.63	0.61	0.36	0.55	0.61
A256		0.18	0.25	0.33	0.40	0.39	0.49	0.29	0.42	0.54	0.60	0.69	0.77
Mandrill		0.27	0.28	0.32	0.33	0.36	0.39	0.53	0.53	0.60	0.56	0.57	0.62
Pepper		0.20	0.20	0.23	0.27	0.32	0.39	0.37	0.40	0.46	0.51	0.62	0.64
Zelda		0.17	0.17	0.24	0.25	0.28	0.32	0.25	0.43	0.40	0.46	0.51	0.54

Table 4.2 Average value of γ

Generalized Gaussian		Gamma	
	γ		γ
$0 \leq \alpha \leq 0.1$	0.25	$\alpha = 0$	0.43
$0.1 < \alpha \leq 0.2$	0.30	$0 < \alpha \leq 0.2$	0.50
$0.2 < \alpha \leq 0.3$	0.34	$0.2 < \alpha < 0.5$	0.60
$0.3 < \alpha \leq 0.4$	0.37		
$0.4 < \alpha < 0.5$	0.42		

For periodic functions, the sequency is one half the number of sign changes per period. If the function is aperiodic, the sequency is one half the number of sign changes per unit time. The Hadamard transform coefficients and thus the HNPT coefficients can be reordered with sequencies arranged in increasing order. The HNPT of a one dimensional data sequence is defined as

$$q(n) = \psi(\alpha)p(n) \qquad n = 0,1,\ldots N - 1 . \qquad (4.5)$$

The relationship between the non-sequency ordered coefficients q(n) and the sequency ordered coefficients q_s(n) is given by

$$q(n) = q_s(b\langle n \rangle) \qquad n = 0,1,\ldots N - 1 . \qquad (4.6)$$

where $\langle n \rangle$ is the bit-reversal of the binary representation of n and $b\langle n \rangle$ is the Gray code-to-binary conversion of $\langle n \rangle$. For example, when $N = 4$,

$$q(0) = q_s(0) \qquad q(1) = q_s(3) \qquad q(2) = q_s(1) \qquad q(3) = q_s(2). \qquad (4.7)$$

For two-dimensional data, the rows can be reordered with increasing sequency followed by reordering the columns.

The histogram of the first row and the first column of the sequency ordered coefficients is compared to the same density functions discussed earlier. In this case, the generalized gaussian provided a better fit to the low sequency data. For $\gamma = 0.5$ and $\gamma = 0.75$, the quantizers listed in [48] can be used. For $\gamma = 1.0$, the pdf is Laplacian and the appropriate quantizers can be found in [21]. The results are summarized in Table 4.3.

Table 4.3 Shape Parameter for Low Sequency HNPT Coefficients

Generalized Gaussian	
	γ
$0 \leq \alpha \leq 0.2$	0.50
$0.2 < \alpha \leq 0.4$	0.75
$0.4 < \alpha \leq 0.5$	1.00

4.2.1 Hadamard Subband Coding

Using the same histogram fitting techniques with the Hadamard subband coding method described in Section 3.2.2 reveals that the generalized Gaussian pdf provides a good fit with the subband histogram data using a shape parameter value of $\gamma = 0.5$. The same set of quantizers used for wavelet subband coding in [47] can also be used with Hadamard subband coding.

4.3 Lloyd-Max Quantizers

Lloyd-Max (LM) quantizers are optimized to yield the minimum mean-squared error for a specified number of reconstruction levels [21]. The quantization error between a quantized signal y and the original signal x is given by

$$q = y - x .$$ (4.8)

Using quantization error variance as an error criterion, the following equation must be minimized.

$$\sigma_q^2 = \sum_{k=1}^{N} \int_{x_k}^{x_{k+1}} (x - y_k)^2 p_x(x) dx$$ (4.9)

The x_k's are the decision levels and the y_k's are the reconstruction levels.

$$
\begin{aligned}
x_{1,opt} &= -\infty \\
x_{k,opt} &= \tfrac{1}{2} * (y_{k,opt} + y_{k-1,opt}) \qquad k = 2,3,\ldots,N \\
x_{N+1,opt} &= \infty
\end{aligned}
$$ (4.10)

and

$$y_{k,opt} = \frac{\int_{x_{k,opt}}^{x_{k+1,opt}} x\, p_x(x) dx}{\int_{x_{k,opt}}^{x_{k+1,opt}} p_x(x) dx} \qquad k=1, 2, \ldots, N .$$ (4.11)

The optimum values of x_k and y_k are solutions to the nonlinear equations above. One method of solving these equations begins by assigning the initial values of y_k and using Equation (4.10) to compute the decision levels. A new set of reconstruction levels is calculated and the process is repeated until the mean-squared error between successive iterations is below a specified threshold. By minimizing the mean-squared error, the Lloyd-Max quantizer design allows more decision levels in regions where the signal's pdf is large. One example of a seven level Lloyd-Max quantizer for the gamma pdf in

Equation (4.3) is given in Table 4.4 where k is the level number and y_k is the reconstruction level. The quantizer specified is for zero mean and unity variance with the decision levels centered between the reconstruction levels. Other quantizer designs for the gamma distribution are found in [23] and [34]. The results presented here are similar with some variations due to differences in the stopping criteria. In addition to quantizers designed for a shape parameter of $\gamma = 0.5$, Appendix B also lists quantizers designed for $\gamma = 0.6$.

Since the HNPT coefficient histogram changes shape with changing values of α, these quantizers will only be used to compress the data when $\alpha < 0.5$. For values of $\alpha > 0.5$, a significant portion of the original image content is still present in the transform coefficients and the data is not decorrelated enough for good compression results.

Table 4.4 Lloyd-Max Reconstruction Levels
for Gamma pdf with $\gamma = 0.6$

k	y_k
1	-3.589
2	-1.726
3	-0.674
4	0.000
5	3.589
6	1.726
7	0.674

4.4 Uniform Threshold Quantizers

Since the HNPT coefficients histogram contains such a sharp center peak (see Figure 3.1), symmetric uniform threshold quantizers (UTQ's) or "dead zone" quantizers provide another quantizer option. UTQ's are symmetric uniform quantizers with the reconstruction levels at the midpoints of the threshold intervals [9][45]. Dead zone quantizers are a variant of uniform threshold quantizers that have a center dead zone with a larger width than the fixed threshold interval. Generally the region around the origin is twice the size of the other intervals. Increasing the size of the dead zone minimizes quantization error noise in the high frequency subbands and has little effect on perceptual quality [15]. One advantage of these quantizers is their ease of implementation. The width of the dead zone and the quantization step size are the only information needed for coding and decoding.

Several researchers have presented results demonstrating that the performance of uniform threshold quantizers is close to that of a optimum entropy constrained quantizer [5] [9] [45]. Berger [5] has shown that a uniform threshold quantizer is optimal for exponential and Laplacian probability density functions while Farvardin and Modestino [9] compare the performance of optimum quantizers and uniform quantizers for several generalized distributions. In both cases, rate-distortion curves provide a means of evaluating quantizer performance. An optimum quantizer is defined as a quantizer that minimizes the distortion (mean-squared error in this case) subject to an entropy constraint. The distortion is defined in Equation (4.9).

$$D = \sum_{k=1}^{N} \int_{x_k}^{x_{k+1}} (x - y_k)^2 p_x(x) dx \qquad (4.12)$$

Like the Lloyd-Max quantizers described in the previous section, the x_k's are the decision

levels and the y_k's are the reconstruction levels. The output entropy rate is

$$H = -\sum_{k=1}^{N} p_k \log_2 p_k \quad bits/sample \tag{4.13}$$

where p_k is the probability that reconstruction level y_k will occur. Finding the optimal

quantizer involves solving a set on simultaneous nonlinear equations. Farvardin and

Modestino show that uniform threshold quantizers closely approximate the rate-distortion

behavior of optimal quantizers.

Figure 4.2 shows the rate-distortion performance of the uniform threshold

quantizers designed for the gamma pdf. The rate-distortion performance curves are

obtained by varying the quantizer step size and calculating the distortion and entropy

associated with an N level quantizer. The optimum N level uniform threshold quantizer

corresponds to the step size resulting in the minimum distortion. Also included are the

Gish-Pierce asymptotic results [16]. Gish and Pierce demonstrate that as distortion

approaches zero (large values of N), the optimum quantizer with an entropy constraint

should tend toward a uniform quantizer and that rate and distortion are related by

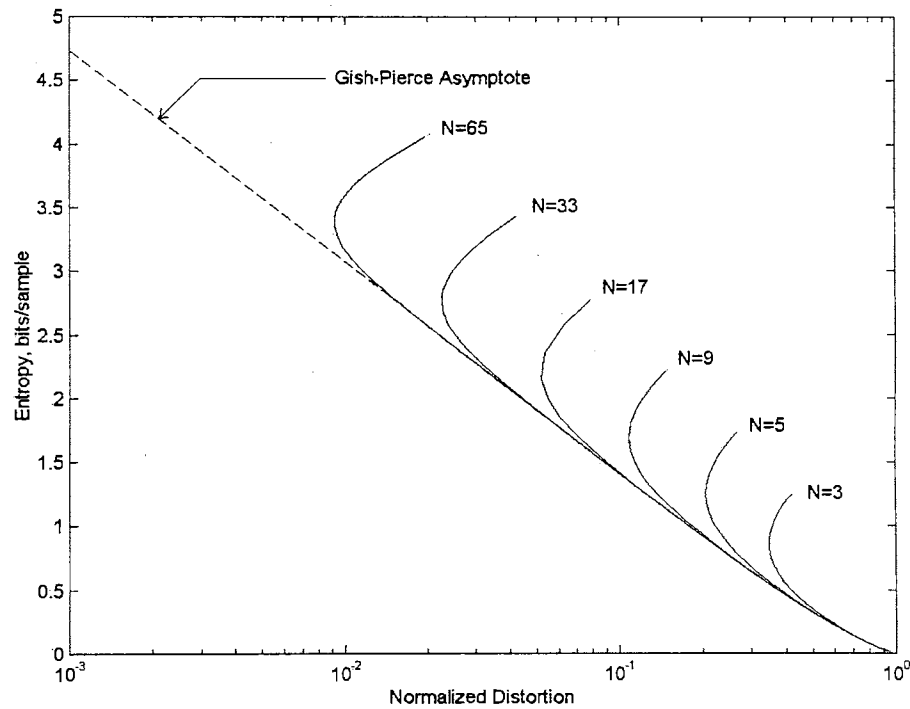Equation (4.14).

$$D(H_O) = \frac{1}{12} 2^{2(h_s - H_O)} \tag{4.14}$$

D is the distortion, $H_O = \log_2 N$ is the rate, and h_s is the differential source entropy

defined below.

$$h_s = -\int_{-\infty}^{\infty} p_x(x) \log_2 p_x(x) dx \quad \text{bits/sample} \tag{4.15}$$
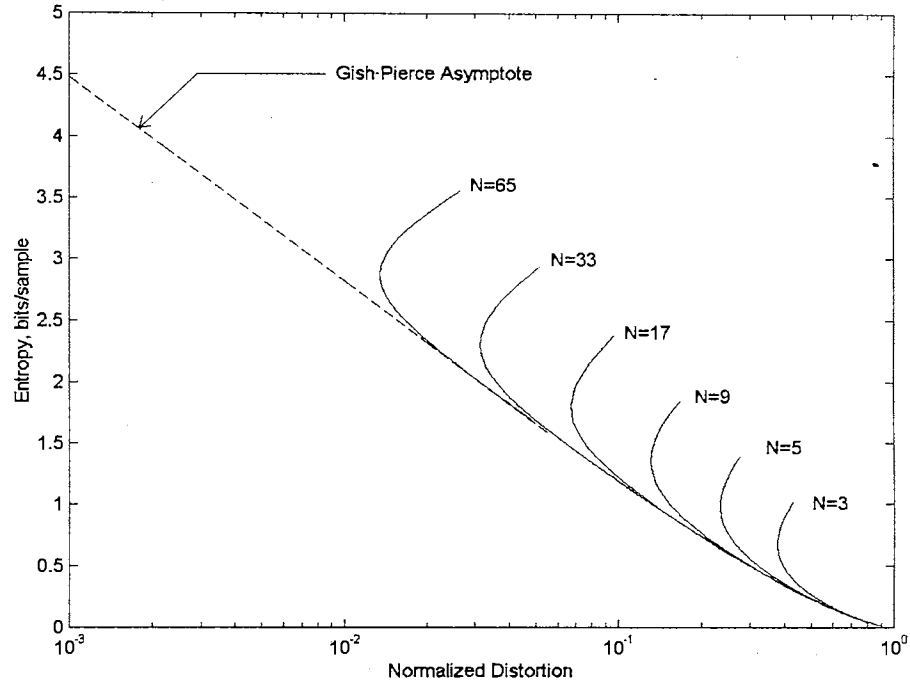
(a)

(b)

Figure 4.2 Performance of Uniform Threshold Quantizer
Gamma Distribution a) $\gamma = 0.5$ b) $\gamma = 0.6$

For the gamma density function with an arbitrary γ, h_s is given by Equation (4.16) where ψ is known as either Euler's psi function or the digamma function.

$$h_s = \frac{1}{\ln 2}\left(-\ln\frac{b}{2\Gamma(\gamma)} + (1-\gamma)\psi(\gamma) + \gamma\right) \text{bits/sample} \qquad (4.16)$$

4.5 Implementation

Figure 4.3 shows the block diagram of the encoding system for image compression using the HNPT. The input image is transformed using the HNPT. In order to reduce the bit rate, the low sequency coefficients and the high sequency coefficients are encoded separately with their respective quantizers. For the high sequency coefficients, only the coefficients with nonzero quantized values are transmitted along with a map of their positional information. The quantization information is further compressed by using adaptive Huffman encoding [12] [13]. In addition to the quantized data, the low and high sequency means and variances are transmitted as overhead information. Also included in the overhead are the value of α, the number of quantization levels, and a 2 x 2 block of the lowest sequency coefficients. Assuming two bytes for each overhead parameter and four bytes for the low uncompressed low sequency coefficients, the overhead information corresponds to transmitting an additional 0.004 bpp.
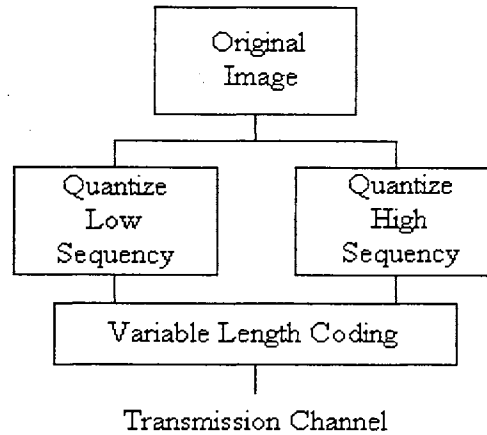
```
                    ┌─────────────┐
                    │   Original  │
                    │    Image    │
                    └─────────────┘
              ┌────────────┴────────────┐
      ┌───────────────┐         ┌───────────────┐
      │   Quantize    │         │   Quantize    │
      │     Low       │         │     High      │
      │   Sequency    │         │   Sequency    │
      └───────────────┘         └───────────────┘
          └─────────────┬──────────────┘
        ┌──────────────────────────────────┐
        │     Variable Length Coding       │
        └──────────────────────────────────┘
                        │
               Transmission Channel
```

Figure 4.3 Block Diagram of HNPT Image Encoder

4.6 Compression Results and Comparison to Other Coding Techniques

This section presents the compression results using both the Lloyd-Max quantizers and the uniform threshold quantizers described earlier. Coding results are presented for the following images *Goldhill*, *C256*, and *Zelda*. The reconstructed images are evaluated in terms of signal-to-noise ratio and the average bits per pixel (bpp). For all examples presented, the HNPT weighting coefficient is $\alpha = 0.2$ and the low sequency coefficients are encoded using the generalized gaussian Lloyd-Max quantizer with $\gamma=0.5$.

Figure 4.4 compares the original *Goldhill* and *C256* images with reconstructed images at two different bit rates. For the low sequency coefficients, 31 quantization levels were used. The different bit rates are due to the type of quantizer used with the high sequency coefficients. Figure 4.4b was obtained using a Lloyd-Max quantizer with 31 levels. The Lloyd-Max quantizer resulted in bit rates of 2.77 bpp and 2.99 bpp and peak signal-to-noise ratios of 25.29 dB and 26.24 dB for *Goldhill* and *C256* respectively.

When the UTQ (N = 33) was used, both the compression ratio and the signal-to-noise ratio increased. For *Goldhill*, the bit rate decreased to 1.70 bpp and the PSNR increased slightly to 25.43 dB. While for *C256*, the bit rate decreased to 1.46 bpp and the PSNR increased to 26.67 dB.

Understanding the coding artifacts caused by the HNPT compression scheme will assist in the development of a POCS based restoration algorithm. The artifacts introduced into the reconstructed images are evident in Figure 4.4. The reconstructed images all contain blocking artifacts caused by the periodic structure of the Hadamard transform. Figure 4.5 shows the difference images between the original images of Figure 4.4a and the reconstructed images of Figure 4.4c. The difference images reveal that the greatest source of error in the reconstructed image is due to the current method of quantizing the low sequency coefficients. There is no evidence of missing edges (high frequency information). The difference image contains large blocks of apparently uniform magnitude values. These blocking artifacts present additional reasons for improving the coding of the low sequency coefficients.

Figure 4.6 presents the results for encoding *Zelda* at a compression ratio of about 12:1. The only difference in the encoder is the quantizer used for the high sequency coefficients. Quantizer levels were adjusted to achieve approximately the same compression ratio using the two different methods. Again, the visually distracting blocking artifacts are present. Another point of interest is the subjective quality of the two reconstructed images. The result from the Lloyd-Max quantizer appears grainier while the UTQ encoded result has smoother appearing blocks. Also, the PSNR for the UTQ reconstructed image is higher at 22.18 dB compared to 18.07 dB. This is a result of

being able to use more high sequency quantization levels to achieve a similar bit rate to the Lloyd-Max quantizer. The bit rate and PSNR results for Figures 4.4 and 4.6 are summarized in Table 4.5.

The HNPT coding results at a compression ratio of 8:1 are compared with equivalent JPEG encoding results. Figure 4.7 demonstrates the typical artifacts introduced by both types of coders at comparable data rates. In this case, JPEG produces a significantly better reconstruction. While the difference in edge quality appears minimal, large blocking artifacts and the grainy image appearance reduces the perceptual quality of the HNPT encoded images.

Table 4.5 Average Bit Rate and PSNR

Picture	Quantizer	N_{LS}	N_{HS}	Bit Rate	PSNR
Goldhill	LM	31	31	2.77 bpp	25.29 dB
	UTQ	31	33	1.46 bpp	25.43 dB
	LM	15	5	1.27 bpp	20.72 dB
	UTQ	31	9	1.06 bpp	21.90 dB
C256	LM	31	31	2.99 bpp	26.24 dB
	UTQ	31	33	1.46 bpp	26.67 dB
Zelda	LM	31	8	0.69 bpp	18.07 dB
	UTQ	31	65	0.68 bpp	22.18 dB
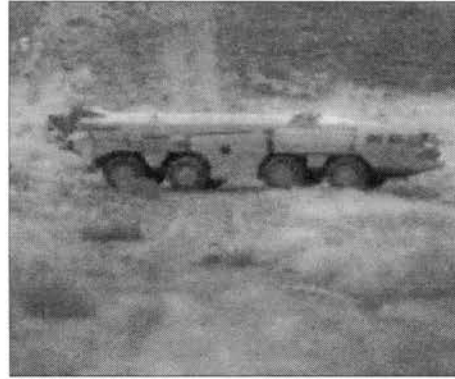
(a)
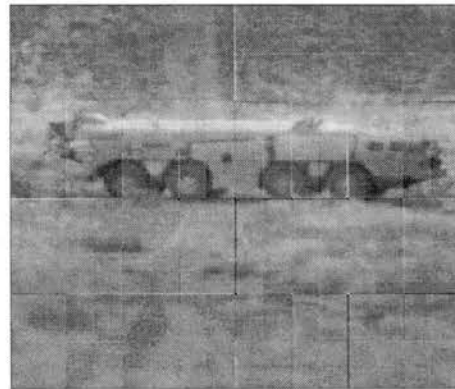
(b)
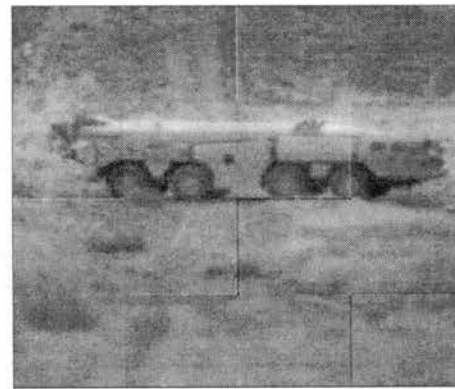
(c)

Figure 4.4 Original and reconstructed *Goldhill* and *C256*
(a) Original images (b) at ~3.0 bpp Lloyd-Max (c) at ~1.5bpp UTQ

Figure 4.5 Original and Difference Images at 1.5bpp

(a)

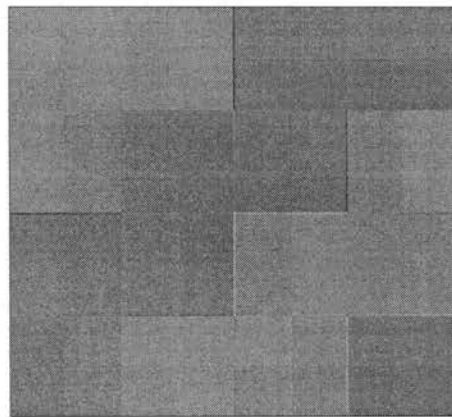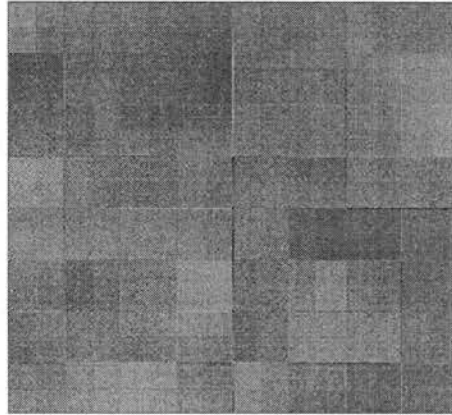
(b)

(c)

Figure 4.6 Original and reconstructed Zelda: (a) Original
(b) at 0.69 bpp Lloyd-Max (c) at 0.68 bpp UTQ
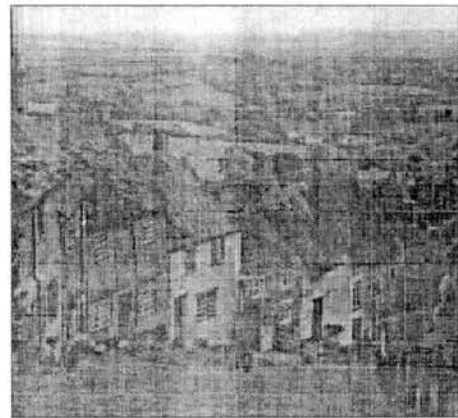
(a)   (b)

(c)   (d)

Figure 4.7 Comparison Between JPEG and HNPT Coding

(a) Original (b) JPEG compressed Goldhill 1bpp

(c) 1.06 bpp UTQ (d) 1.27 bpp Lloyd-Max

4.7 Summary

This chapter presents an encoding scheme using the Hadamard Naturalness-Preserving transform. In order to design quantizers, two possible models for the HNPT coefficient probability density function are presented. With appropriately chosen shape parameters, both the generalized Gaussian and the gamma density functions provide a good fit with the HNPT coefficient data. Both Lloyd-Max quantizer and uniform threshold quantizer designs are presented using the gamma density function.

Understanding the coding artifacts caused by the HNPT will assist in the development of a POCS based restoration scheme. The greatest source of error in the reconstructed image is due to the current method of quantizing the low sequency coefficients because the quantizers are designed for optimum quantization of the high sequency coefficients. As a result, the reconstructed images all contain blocking artifacts caused by the periodic structure of the Hadamard transform. For higher compression ratios, this degradation has an appearance similar to adding salt and pepper noise to the image. Comparisons are also made between the HNPT encoding scheme and baseline JPEG.

CHAPTER 5

HNPT RECONSTRUCTION ALGORITHM

The method of convex projections was introduced to the image processing community by Youla and Webb [57]. In order to apply convex constraints to image recovery problems, known properties (*a priori* knowledge) of the original image must be defined as closed convex sets. These constraints can be used within an iterative algorithm to improve the quality of the received image. Some examples of *a priori* knowledge would be image smoothness (i.e. reduced blocking and ringing artifacts), nonnegativity of pixel values, edge continuity, and preservation of correctly received values. It is important to note that POCS based restoration techniques are applied in the post-processing phase of an image coder. Since several iterations are usually required for convergence of the algorithm, there is a computational cost associated with these methods.

5.1 Definitions

Each desired property of the reconstructed image is defined as a convex set and the resulting image solution is a member of the intersection of all the constraint sets. This section introduces some of the definitions needed to describe a POCS based recovery algorithm.

A Hilbert space H: **H** is an inner product space. For example, $L^2(\Re)$ is the space

of two-dimensional square integrable functions where the inner product is defined by

$$\langle f(x,y), g(x,y) \rangle = \int_{-\infty}^{+\infty}\int_{-\infty}^{+\infty} f(x,y)\, g^*(x,y)\, dx\, dy \qquad (5.1)$$

and g*(x,y) denotes the complex conjugate of g(x,y).

Convex set S: A set S in **H** is convex if and only if for any arbitrary points x_1 and

$x_2 \in S$, the vector $x = \alpha x_1 + (1-\alpha)x_2$ is also in S for $0 \leq \alpha \leq 1$. For any two points x_1 and

x_2 in a convex set, all the elements of the line connecting x_1 and x_2 are also in the set.

Closed set S: A set S in **H** is closed if it contains all of its limit points. The set of

all points in the interval $[\,a, b\,]$ is closed.

Projection onto S: Given $x \in$ **H** and a closed convex set $S \in$ **H**, there exists a $x' \in S$

which is closest to the initial point x ($d = \min \| x\text{-}x' \|$). The distance between x and x' is

a minimum.

Projection operator: P maps x to x'. P: **H** $\rightarrow S$ or $Px \in S$. P is a function or

mapping that assigns to a point x the point $x' = Px \in$ S.

5.2   The Projection Method

Known properties of a data set are defined as constraints which belong to some

closed convex set S_i. For m known properties, there exist m convex sets S_i, $i=1,2, \ldots m$.

The projection of a function $f \in \mathbf{H}$ onto S_i forces f to lie on the intersection, ($f \in S_\cap = \bigcap_{i=1}^{m} S_i$) of these sets. The projection operator P_i projects f onto the desired constraint set S_i. By alternately projecting onto each convex set, every iteration brings f closer to the data estimate that is common to all the sets as is shown in Figure 5.1.
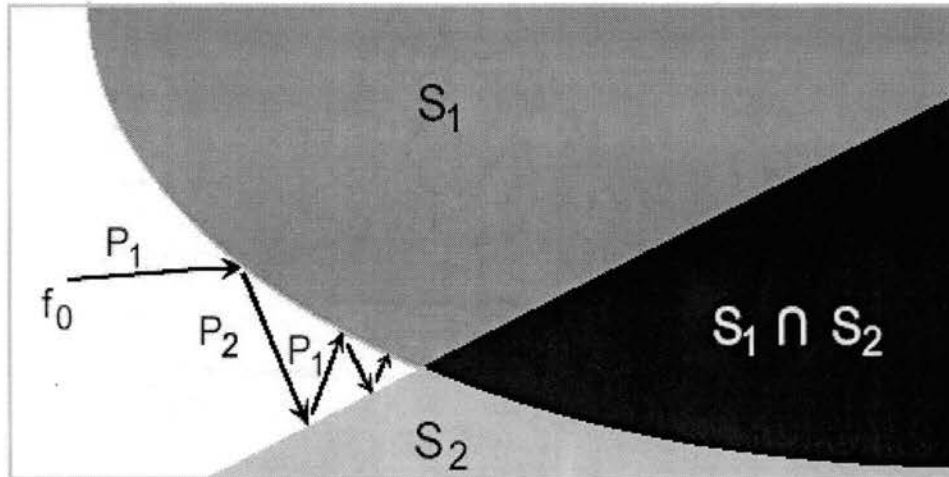
Figure 5.1 Illustration of POCS Technique

The restoration procedure begins with an initial estimate of the original function f_0 where f_0 may lie outside all of the convex sets S_i. Each iteration projects the previous estimate onto each of the convex sets and generates a new estimate.

$$f_i = P_m P_{m-1} \ldots P_2 P_1 f_{i-1} \qquad i = 1, 2, \ldots m \tag{5.2}$$

Youla and Webb show that if two convex sets intersect, convergence will occur [56]. Convergence is typically measured by a closeness metric such as mean-square error or maximum absolute pixel difference. If the constraint sets do not intersect, the solution will oscillate between a point in each set. The convergence point will be unique only if

the sets' intersection, $S_\cap$, contains a single point. Otherwise, any solution in the intersection is considered feasible.

The procedure to implement an image recovery algorithm using POCS is described below.

- Formulate *a priori* knowledge in the form of convex sets. S_i, $i = 1, 2, \ldots, m$

- Develop the corresponding projection operators, P_i.

- Implement Equation (5.2) until the desired stopping criterion $d(f_i, f_{i-1})$ is met.

5.3 Convex Sets and Projection Operators

The HNPT signal reconstruction problem can be described as that of signal reconstruction from partial transform domain information. This section provides a review of the projection operators to be used from Chapter 3 and their corresponding convex constraint sets. A nonexpansive projection operator, P_i, can be associated with each constraint. The projection operator maps all images which violate the constraint onto S_i. Prior knowledge about desired image properties is used along with information about the HNPT coefficients. Typical images have the following properties:

- Pixel limits – the restored pixel values should lie in the range [0,255]

- Consistency with known values – correctly received values are unchanged

- Smoothness – the recovered image should be smooth to reduce blocking artifacts.

After applying the HNPT to image data, there remains some correlation between transform coefficients. This correlation exists because the HNPT is a hybrid transform which contains a portion of the original image and also because the Hadamard transform is not the ideal transform for decorrelating a signal (The Karhunen-Loeve Transform is

optimum based on the mean-square error criterion [2]). Also, the distribution of the high sequency HNPT coefficients is known to be the gamma distribution. Using this knowledge, correctly received coefficients can be used to reconstruct lost values. The following convex sets and projection operators are used for HNPT reconstruction.

1) S_L : The set of $N \times N$ images whose pixel values lie in a closed interval $[a,b]$

$$S_L = \left\{ f \in \Re^{N^2} \middle| a \le f_{i,j} \le b \right. \tag{5.3}$$

where i,j denotes pixel indices and $[a,b] = [0, 255]$. Any pixel that lies outside the valid intensity range is projected to the appropriate range boundary. The projection for limiting pixel values is defined below.

$$P_L f = \begin{cases} a & f_{i,j} < a \\ f_{i,j} & a \le f_{i,j} \le b \\ b & f_{i,j} > b \end{cases} \tag{5.4}$$

Equation (5.4) can also be used to ensure valid quantization ranges where a and b are the quantization interval boundaries.

2) S_C: The set of images with some pixel intensities equal to known values

$$S_C = \left\{ f \in \Re^{N^2} \middle| f_{i,j} = k_{i,j} \quad (i,j) \in M \right. \tag{5.5}$$

where $k_{i,j}$ are the known pixel values in an index set M. In a practical communications channel, packetization of the encoded data allows for synchronization of the bitstream, prioritization of the packets, and progressive transmission of the data. Since the data is transmitted in a specified order, the location of lost packets can be determined [18] [43]. The definition of P_L is expanded so that neighboring pixel values remain the same and only the pixel values in the damaged areas are altered. The projection operator P_C

ensures that correctly received values are not altered by the restoration process and is described by

$$P_C f = \begin{cases} k_{i,j} & (i,j) \in M \\ f_{i,j} & otherwise. \end{cases} \quad (5.6)$$

M denotes the location of the correctly received pixel values. P_L and P_C can be combined into one operator or they can be applied independently.

3) S_T : The set of images with transform coefficients equal to known values.

$$S_T = \left\{ f \in \Re^{N^2} \mid [Tf]_{i,j} = z_{i,j} \quad (i,j) \in M \right. \quad (5.7)$$

where T is a linear transform operator, $[Tf]_{i,j}$ are the transform coefficients, and $z_{i,j}$ are known coefficients in an index set M. In this case, T is the two-dimensional $N \times N$ HNPT. The projection operator P_T onto S_T is

$$[P_T Tf] = \begin{cases} z_{i,j} & (i,j) \in M \\ [Tf]_{i,j} & otherwise \end{cases} \quad (5.8)$$

4) S_S : The set of images without blocking artifacts.

$$S_S = \left\{ f \in \Re^{N^2} \mid f \text{ is smooth at block boundaries} \right. \quad (5.9)$$

The projection operator P_T can be used to impose smoothness where T is the two-dimensional discrete Fourier transform. With this definition, an image is lowpass filtered and any coefficients outside a specified frequency are zeroed. Yang *et. al.* provide a mathematical definition specifically for smoothness at block boundaries [51] [52].

$$S_S = \left\{ f \in \Re^{N^2} \mid \| Qf \| \leq E \right. \quad (5.10)$$

Q is a linear operator such that Qf is the difference between the adjacent columns at block boundaries where f_i denotes the ith column of the image. The norm of Qf, $\| Qf \|$, is a measure of the intensity variation at the block boundaries.

$$Qf = \begin{bmatrix} f_8 - f_9 \\ f_{16} - f_{17} \\ \vdots \\ f_{248} - f_{249} \end{bmatrix} \text{ and } \| Qf \| = \left[\sum_{i=1}^{31} \| f_{8\cdot i} - f_{8\cdot i+1} \|^2 \right]^{\frac{1}{2}} \tag{5.11}$$

E is a scalar upper bound for the set and is a measure of the intensity variation between adjacent columns of the entire image.

$$E = \frac{1}{7} \sum_{k=1}^{7} S_k \tag{5.12}$$

f' denotes the blocky image and S_k is defined as

$$S_k \equiv \left[\sum_{i=1}^{31} \| f'_{8\cdot i+k} - f'_{8\cdot i+k+1} \|^2 \right]^{\frac{1}{2}} \qquad k = 1, 2, \ldots, 7. \tag{5.13}$$

For a 256 x 256 image with 8 x 8 blocks, the projection onto S_S is given by

$$\tilde{f} = P_S f = \begin{cases} \tilde{f}_i = \alpha \cdot f_i + (1-\alpha) \cdot f_{i+1} \text{ and} \\ \tilde{f}_{i+1} = (1-\alpha) \cdot f_i + \alpha \cdot f_{i+1} & \text{for } k = 1, 2, \ldots, 31 \text{ and } i = 8 \cdot k \\ \text{otherwise } \tilde{f}_i = \tilde{f}_i \end{cases} \tag{5.14}$$

where $\alpha = \frac{1}{2} \left[\frac{E}{\| Qf \|} + 1 \right]$. P_S can be applied to the image rows in a similar fashion.

5.4 Implementation

For the following examples, random transform coefficients (not packets) are dropped. The location of the lost data is known and the transform coefficients are

initialized to zero at the decoder. This assumption is consistent with the transmission protocols available in ATM networks [41]. For packet transmission, data is sent in a predetermined order. Additionally, interleaving the data prevents losing large contiguous areas of data.

Transform coefficients that are lost in transmission can be replaced with an estimate obtained from neighboring values using linear interpolation. Lost coefficients can have at most four correctly received neighbors. The reconstructed coefficient $\hat{c}_{i,j}$ is given by

$$\hat{c}_{i,j} = Fc_{i,j} = w_1 c_{i,j-1} + w_2 c_{i-1,j} + w_3 c_{i+1,j} + w_4 c_{i+1,j-1}. \tag{5.15}$$

High sequency coefficients with the largest number of correctly received neighbors are reconstructed first. These new values are then used to reconstruct the coefficients with fewer available neighbors. If a neighboring coefficient is missing, the corresponding weight is set to zero until the adjacent coefficient is reconstructed. Low sequency coefficients are reconstructed using only the two largest neighbor coefficients. Using F and the projection operators described earlier, Equation (5.2) is written as

$$f_k = P_L P_C P_S F \, f_{k-1} \tag{5.16}$$

Image restoration at the decoder is performed iteratively by repeated application of the projections defined above. Also note that F is not a convex projection operator but it does have properties that are useful in the restoration process. If F is nonexpansive, it will not interfere with the convergence of the algorithm. The algorithm defined by Equation (5.16) can be better described as a constrained minimization algorithm employing POCS techniques. Mean-square error (MSE) is used as a distance metric between iterations to determine convergence.

5.5 Image Reconstruction Results

In this section, experimental results are presented for the POCS reconstruction techniques. Figures 5.3 through 5.6 demonstrate the performance of the reconstruction algorithm for random coefficient loss with loss percentages ranging from 10% to 30%. The reconstruction technique is evaluated by computing the peak signal-to-noise ratio. Figure 5.2 presents the original images for comparison purposes. Sample reconstructed images for *Goldhill* and a 256 x 256 section of *Zelda* are shown in Figures 5.3 and 5.4. For both test images, 10% of the transform coefficients are randomly lost. Figures 5.3d and 5.4d demonstrate the convergence of the algorithm in less than 10 iterations. Figures 5.4 and 5.5 are a military vehicle test image provided by Sandia National Laboratories. Figure 5.4 demonstrates the results for 10% coefficient loss and Figure 5.5 provides reconstruction examples for 20% and 30% coefficient loss.

The application of a POCS based restoration scheme improved the quality of the reconstructed images. In terms of visual quality, all the reconstructed images exhibit some blocking artifacts which are caused by the low sequency reconstruction. To determine the effectiveness of the smoothing constraint, Equation (5.16) was implemented without P_S. For the examples shown, the addition of P_S improved the final PSNR by .05 dB to .15 dB and reduced but did not completely eliminate the blocking artifacts. Signal-to-noise ratios are much improved for all the reconstructed images. The PSNR results are summarized in Table 5.1.

With its variety of complicated textures and edge information, *Goldhill* provides a challenging test case. In general, high frequency details are preserved while low frequency regions are not reconstructed well by the current algorithm. Both *Goldhill* and

Zelda demonstrate the reconstruction errors encountered in low frequency regions. The visual effect on the images is that of adding salt and pepper noise. Reduction of this error would increase signal-to-noise ratios.

The results for *C256* are more promising. The vehicle image has a different texture content than the standard test images. The Sandia images have a low detail, almost uniform background texture. Despite high loss, the vehicle images in Figure 5.6 are recognizable and larger vehicle features such as wheels are preserved. With 30% coefficient loss, the road disappears into the background and smaller windows and structures are lost. Figure 5.7 presents the PSNR results for loss percentages ranging from 5% to 30% for *C256*, *Cameraman*, and *Goldhill*.

Table 5.1 Reconstruction Performance

Picture	% Lost Coefficients	Initial PSNR	Final PSNR
Goldhill	10.4%	15.9 dB	26.0 dB
Zelda	10.3%	17.1 dB	24.0 dB
C256	10.4%	16.9 dB	30.6 dB
C256	21.3%	13.8 dB	28.0 dB
C256	30.0%	12.3 dB	25.6 dB

(a)

(b)
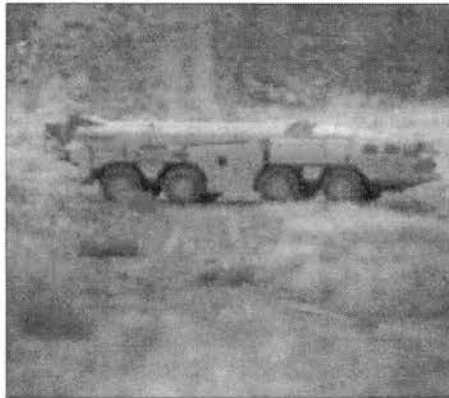
(c)

Figure 5.2 Original Images: (a) Goldhill
(b) Zelda subimage (c) C256 vehicle

(a)

(b)

(c)

(d)

Figure 5.3 *Goldhill* with 10% Random Loss : (a) Initial image, PSNR =15.9 dB (b) First iteration of reconstruction algorithm (c) Final reconstructed image, PSNR = 26.0 dB (d) Demonstration of convergence

(a)

(b)

(c)

(d)

Figure 5.4 *Zelda* Subimage with 10% Random Loss : (a) Initial image, PSNR =17.1 dB
(b) First iteration of reconstruction algorithm (c) Final reconstructed image, PSNR = 24.0
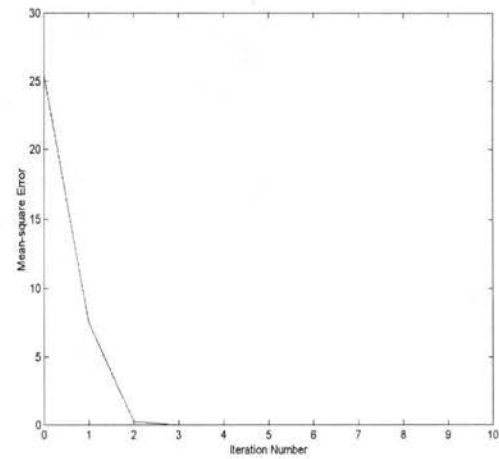dB (d) Demonstration of convergence

(a)

(b)

(c)
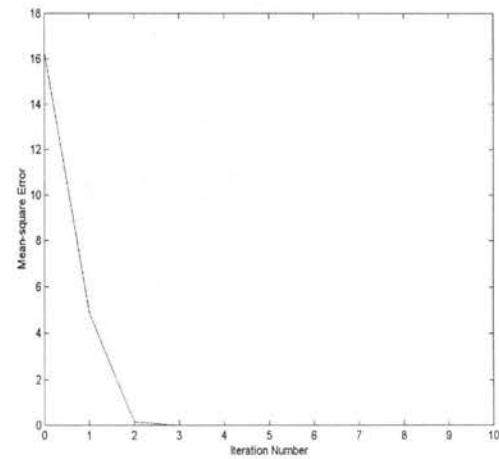
(d)

Figure 5.5 *C256* Vehicle Image with 10% Random Loss : (a) Initial image, PSNR =16.9 dB (b) First iteration of reconstruction algorithm (c) Final reconstructed image, PSNR = 30.6 dB (d) Demonstration of convergence
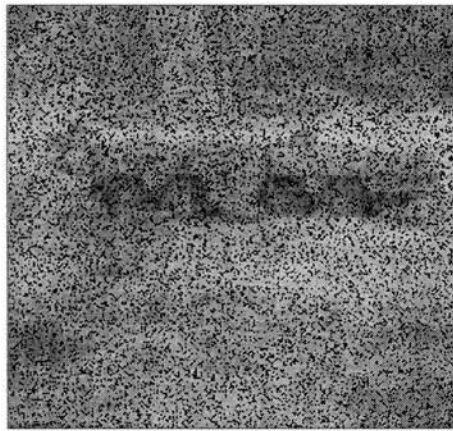
(a)
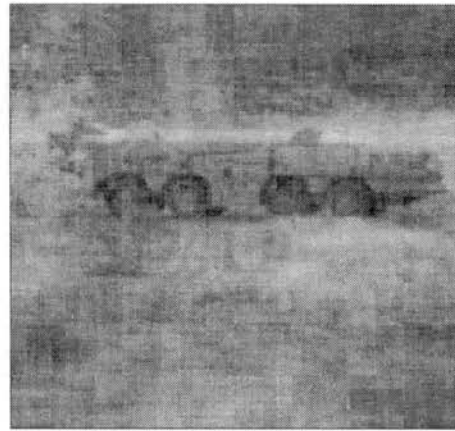
(b)

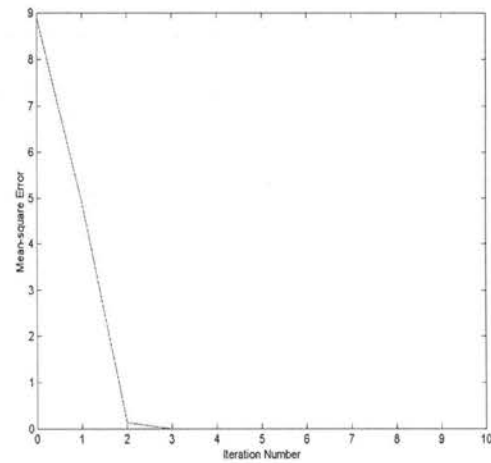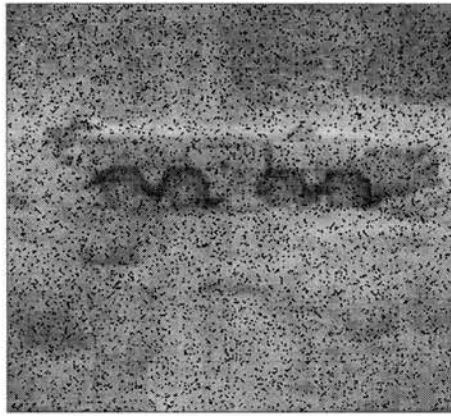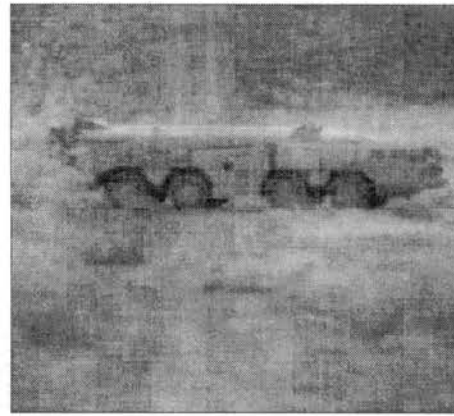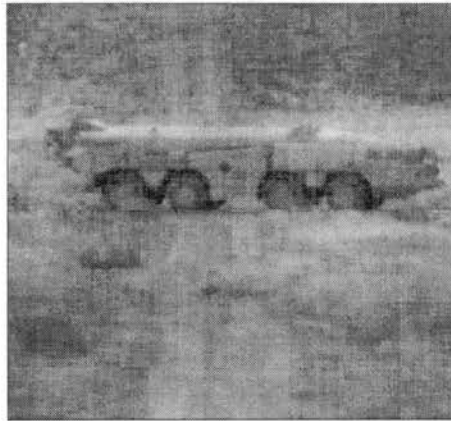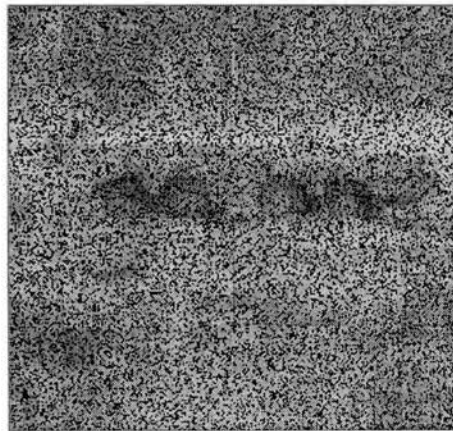
(c)
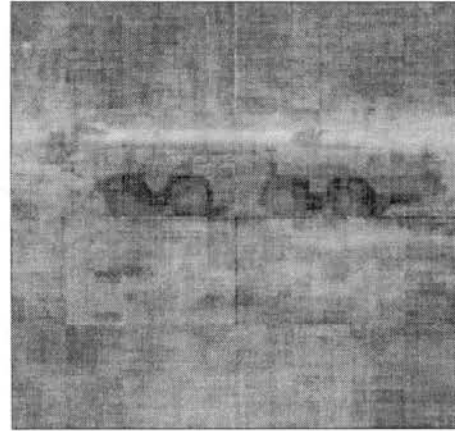
(d)

Figure 5.6 *C256* Vehicle Image : (a) Initial image with 20% random loss, PSNR =13.8 dB (b) Final reconstructed image, PSNR = 28.0 dB (c) Initial image with 30% random loss, PSNR = 12.3 dB (d) Final reconstructed image, PSNR = 25.6 dB
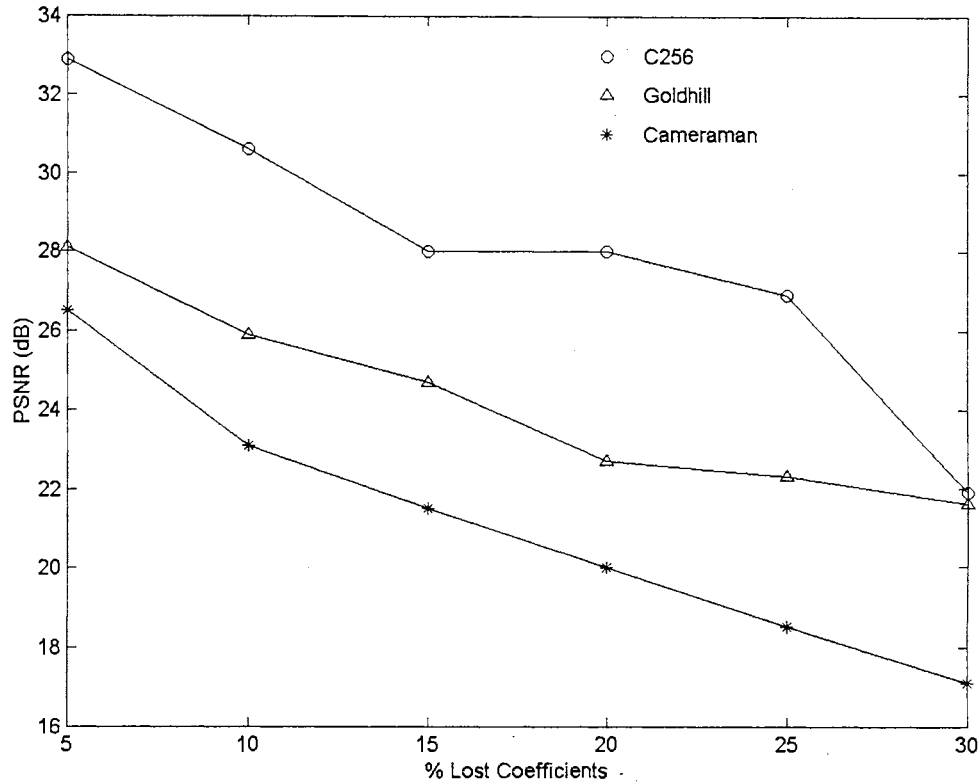
Figure 5.7 Reconstruction Performance

5.6 Packetization Assumptions

In Chapter 3 some basic packet network assumptions are presented. This section reviews those assumptions and describes some assumptions directly related to HNPT coding and reconstruction. The following network properties are assumed:

- Coefficient data is transmitted in a predetermined order. Thus, insertion of sequence numbers provides a method for identification of lost packets.

- Interleaving the data before packetization avoids the problem of loss in adjoining areas of an image.

Segmentation of the data can occur in either the spatial or the frequency domain. By sequency ordering the HNPT coefficients before transmission, packetization occurs in the frequency domain and interleaving is achieved naturally. Loss of a packet would correspond to loss of frequency information from different spatial regions in the image. The effect would be similar to the random coefficient loss simulated in Section 5.4

5.7 Summary

An image reconstruction technique employing projections onto convex sets is proposed to improve the quality of HNPT coded images degraded by random coefficient loss. Prior knowledge about desired image properties is used along with information about the HNPT coefficients. Specific constraints such as limiting pixel values, preservation of correctly received values, and image smoothness are combined with linear interpolation for reconstruction of lost coefficients. The techniques presented improve the peak signal-to-noise ratio and converge within 5 iterations.

CHAPTER 6

CONCLUSIONS AND FUTURE WORK

This chapter summarizes the research presented in this thesis and highlights the major contributions of this research. Future work on improving the compression and restoration algorithms is also discussed.

6.1 Summary and Conclusions

The Hadamard Naturalness-Preserving Transform has been proposed for possible use in situations where the communications channel results in severely degraded output images due to noise and/or jamming. An image coder using the HNPT along with a decoder-based restoration scheme using convex projections is presented. The algorithms are designed for use in packet-based transmission systems with low bandwidth and computational power available at the decoder.

In order to design quantizers, histogram fitting techniques were utilized to determine the shape of the HNPT coefficient histogram. Both Lloyd-Max quantizers and uniform threshold quantizers have been designed for use in encoding HNPT coefficients. The current quantizers perform well in quantizing the high sequency coefficients.

When data is corrupted by noise or lost during transmission, the received data cannot completely describe the original image content. A POCS based reconstruction

scheme uses prior knowledge about natural images along with the received data to reconstruct an estimate of the original image. The reconstruction algorithm also allows *a priori* knowledge about characteristics of HNPT transformed data to be incorporated into the restoration process. The restoration algorithm described in this thesis proved successful in improving visual quality even in example cases where thirty percent of the transform coefficients are lost. By enforcing consistency with known transform coefficients, corrupted coefficients were brought closer to an estimate of their original magnitude. The restoration algorithm improved the quality of degraded HNPT coded images within 5 iterations.

6.2 Contributions

The following are major contributions of this research. The shape of the HNPT coefficient histogram has been characterized for weighting constant values over the range $0 \leq \alpha < 0.5$. For appropriately chosen shape parameters, both the generalized Gaussian probability density function and the gamma density function provide a good fit with the high sequency HNPT data. The gamma density function shape parameter has less variation in its shape parameter values and thus is chosen for modeling the HNPT coefficients. Both Lloyd-Max quantizers and uniform threshold quantizers are designed for the gamma distribution using the shape parameter values of either $\gamma = 0.6$ or $\gamma = 0.5$. The major source of error in the compressed images is a result of the current method of selecting and quantizing the low sequency coefficients. Although the HNPT coded images do not exhibit the same visual quality as JPEG coded images, compression results demonstrate the effectiveness of the high sequency coefficient quantizers.

The performance of the HNPT reconstruction algorithm works well for the standard test images and is particularly effective for images from Sandia's linear array imaging system. The method of projections onto convex sets allows for the description of available information in the form of convex constraint sets and also allows for an iterative reconstruction algorithm. The HNPT encoder is not required to send any additional information. All computation is performed at the decoder. The POCS reconstructed images have better visual quality and higher signal-to-noise ratios than those reconstructed from partially received HNPT coefficient data. Using *C256* as an example, a coefficient loss of 30% results in an initial PSNR of 12.3 dB. After application of the POCS reconstruction algorithm, the PSNR is 25.6 dB. The disadvantage of using the convex projections approach to reconstruction is the delay involved in the repeated iteration of the constraints.

6.3 Suggested Future Work

Periodic blocking artifacts in both the HNPT compressed images and the POCS reconstructed images are due to the current method of determining the location of the low sequency coefficients. Low sequency coefficients are generally located in the first row and first column of the sequency ordered HNPT coefficients. This assumption works well but does not completely determine the location of all the higher magnitude coefficients. The HNPT encoder can be improved by including more coefficients in the low sequency quantization. A small amount of additional overhead would be needed to transmit this information.

The current smoothness constraint only operates on the blocking artifact boundary. This approach works well but does not completely eliminate the blocking artifact. Smoothness sets utilizing image statistics from a larger local neighborhood or the addition of a lowpass filter can be utilized to reduce the blocking artifacts. If the filter is nonexpansive, it will not interfere with the convergence of the POCS algorithm. The results in Chapter 5 are from unquantized coefficients. The same concepts can be extended to quantized values. Additional constraints would take into account quantization interval boundaries and preservation of image edges.

REFERENCES

[1]   E. H. Adelson, E. P. Simoncelli, and R. Hingorani, "Orthogonal pyramid transforms for image coding," *Proc. SPIE*, vol. 845, pp. 50-58, October 1987.

[2]   N. Ahmad and K. R. Rao, *Orthogonal Transforms for Digital Signal Processing*, Springer-Verlag, 1975.

[3]   G. L. Anderson and A. N. Netravali, "Image restoration based on a subjective criterion," *IEEE Trans. Syst. Man Cybern.*, vol. 6, pp. 845-853, 1976.

[4]   D. M. Baylon and J. S. Lim, *Transform/subband Analysis and Synthesis of Signals*, MIT, Cambridge, Mass., Research Laboratory of Electronics, Technical Report, June 1990.

[5]   T. Berger, "Optimum quantizers and permutation codes," *IEEE Trans. Information Theory*, vol. 18, pp. 759-765, Nov. 1972.

[6]   L. H. Croft and J. A. Robinson, "Subband image coding using watershed and watercourse lines of the wavelet transform," *IEEE Trans. Image Processing*, vol. 3, no. 6, pp. 759-771, 1994.

[7]   A. Crosier, D. Esteban, C. Galand, "Perfect channel splitting by use of interpolation, decimation, and tree decomposition techniques," *Proc. of Int. Conf. On Information Sciences/Systems*, Patras, Greece, pp. 443-446, August 1976.

[8]   R. A. DeVore, B. Jawerth, and B. J. Lucier, "Image compression through wavelet transform coding," *IEEE Trans. Information Theory*, vol. 38, no. 2, pp. 719-746, March 1992.

[9]   N. Farvardin and J. W. Modestino, "Optimum quantizer performance for a class on non-gaussian memoryless sources," *IEEE Trans. Information Theory*, vol. 30, no. 3, pp. 485-497, May 1984.

[10] C. R. Fore and R. K. Yarlagadda, "Convex projections restoration of Hadamard naturalness-preserving transform coded images," *Proceedings of IEEE Southwest Symposium on Image Analysis and Interpretation*, pp. 18-22, Tucson, April 1998.

[11] C. R. Fore and R. K. Yarlagadda, "Coding and restoration of Hadamard naturalness-preserving transform coded images," Workshop on Data Compression

Processing Techniques for Missile Guidance Data Links, Redstone Arsenal, Huntsville, December 1998.

[12] R. G. Gallagher, "Variations on a theme by Huffman," *IEEE Trans. Information Theory,* vol. 24, pp. 668-674, Nov. 1978.

[13] A. Gersho and R. M. Gray, *Vector Quantization and Signal Compression*, Kluwer Academic Publishers, Boston, Ma, 1992.

[14] M. Ghanbari and D. E. Pearson, "Probability density functions for Hadamard coefficients in transform television pictures," *Electronics Letters*, vol. 14, no. 8, pp. 252-254, 1978.

[15] H. Gharavi and A. Tabatabai, "Subband coding of monochrome and color images, " *IEEE Trans. Circ. and Syst.,* vol. 35, no. 2, pp. 207-214, Feb. 1988.

[16] H. Gish and J. N. Pierce, "Asymptotically efficient quantizing," *IEEE Trans. Information Theory*, vol. 14, pp. 676-683, Sept. 1968.

[17] R. C. Gonzalez and R. E. Woods, *Digital Image Processing*, Reading, Ma: Addison-Wesley, 1992.

[18] S. S. Hemami and R. M. Gray, "Subband-coded image reconstruction for lossy packet networks," *IEEE Trans. Image Processing,* vol. 6, no. 4, pp. 523-539, April 1997.

[19] ITU-T (formerly CCITT) and ISO/IEC JTC1, "Digital compression and coding of continuous-tone still images," ISO/IEC 10918-1 – ITU-T recommendation T.81 (JPEG), Sept. 1993.

[20] ITU-T (formerly CCITT) and ISO/IEC JTC1, "Generic coding of moving pictures and associated audio recommendation – Part 2: Video," ITU-T recommendation H.262 - ISO/IEC 13818-2 (MPEG-2), Nov. 1994.

[21] N. S. Jayant and P. Noll, *Digital Coding of Waveforms: Principles and Applications to Speech and Video*. Englewood Cliffs, NJ: Prentice-Hall, 1984.

[22] P. W. Jones and M. Rabbani, 1994, "Digital Image Compression," in E. R. Dougherty (ed.) *Digital Image Processing Methods*, pp. 261-325, Marcel Dekker, New York.

[23] P. Kabal, "Quantizers for the gamma distribution and other symmetrical distributions," *IEEE Trans. ASSP*, vol. 32, no. 4, pp. 836-841, August 1984.

[24] A. K. Katsaggelos, "Iterative image restoration algorithms," *Optical Engineering*, vol. 28, no. 7, pp. 735-748, July 1989.

[25] A. K. Katsaggelos, J. Biemond, R. W. Schafer, and R. M. Mersereau, "A regularized iterative image restoration algorithm," *IEEE Trans. Signal Processing*, vol. 39, no. 4, pp. 914-929, April 1991.

[26] M. A. Kohler and R. Yarlagadda, "Naturalness-preserving transform for missing frame compensation," *Proc. IEEE International Symposium on Circ. and Syst.*, May 1999.

[27] S. Mallat and S. Zhong, "Characterization of signals from multiscale edges," *IEEE Trans. Pattern Anal. Machine Intel.*, vol. 14, no. 7, pp. 710-732, July 1992.

[28] A. Manduca, "Interactive wavelet-based image compression with arbitrary region preservation," *Proc. SPIE*, vol. 1808, pp. 410-421, 1992.

[29] P. Noll and R. Zelinski, "Bounds on quantizer performance in the low bit-rate regions," *IEEE Trans. Commun.*, vol. 26, pp. 300-304, Feb. 1978.

[30] A. V. Oppenheim and R. W. Schafer, *Digital Signal Processing*, Englewood Cliffs: Prentice-Hall, 1975.

[31] A. O. Osinubi and R. A. King, "Naturalness-preserving transform (NPT) reconstruction of signals degraded by non-stationary nose processes," *Proc. ICASSP*, vol. 2, pp. 1199-1202, May 1989.

[32] A. O. Osinubi and R. A. King, "One-dimensional Hadamard naturalness-preserving transform reconstruction of signals degraded by nonstationary noise processes," *IEEE Trans. Sig. Proc.*, vol. 40, no. 3, pp. 645-659, March 1992.

[33] A. O. Osinubi, R.A. King, and A. M. Barbarosa, "Predictive naturalness-preserving transform coding of monochromatic images," *Proceedings of the Electrotechnical Conf.*, pp. 292-295, April 1989.

[34] M. D. Paez and T. H. Glisson, "Minimum mean-squared error quantization in speech PCM and DPCM systems," *IEEE Trans. Commun. Tech.*, vol. 20, pp. 225-230, April 1972.

[35] W. B. Pennebaker and J. L. Mitchell, *JPEG Still Image Data Compression Standard*, New York: Van Nostrand Reinhold, 1992.

[36] T. A. Ramstad, S. O. Aase, and J. H. Husoy, *Subband Compression of Images: Principles and Examples*. Amsterdam, The Netherlands: Elsevier Science B. V., 1995.

[37] S. J. Reeves and S. L. Eddins, "Comments on iterative procedures for reduction of blocking effects in transform image coding," *IEEE Trans. Circuits Syst. Video Technol.*, vol. 3, no. 6, pp. 439-440, Dec. 1993.

[38] R. C. Reininger and J. D. Gibson, "Distributions of the two-dimensional DCT coefficients for images," *IEEE Trans. Commun.*, vol. COM-31, pp. 835-839, June 1983.

[39] R. Rosenholtz and A. Zakhor, "Iterative procedures for reduction of blocking effects in transform image coding," *IEEE Trans. Circuits Syst. Video Technol.*, vol. 2, no. 1, pp. 91-95, Mar. 1992.

[40] Eero P. Simoncelli, "Orthogonal Sub-band Image Transforms," Master's Thesis, EECS Department, Massachusetts Institute of Technology, May 1988.

[41] W. Stallings, *Data and Computer Communications*, New Jersey: Prentice-Hall, 1997.

[42] J. K. Su and R. M. Mersereau, "Post-processing for artifact reduction in JPEG-compressed images," *Proc. ICASSP '95*, pp. 2363-2366.

[43] H. Sun and W. Kwok, "Concealment of damaged block transform coded images using projections onto convex sets," *IEEE Trans. Image Processing,* vol. 4, no. 4, pp. 470-477, April 1995.

[44] D. Sundararajan and M. O. Ahmad, "Fast computation of the discrete Walsh and Hadamard transforms," *IEEE Trans. Image Processing,* vol. 7, no. 6, pp. 898-904, June 1998.

[45] N. Tanabe and N. Farvardin, "Subband image coding using entropy-coded quantization over noisy channels," *IEEE Trans. on Selected Areas in Comm.*, vol. 10, no. 5, pp. 926-943, June 1992.

[46] M. Vetterli and J. Kovacevic, *Wavelets and Subband Coding*, Prentice Hall, New Jersey: Englewood Cliffs, 1995.

[47] P. H. Westerink et. al., "Subband coding of images using vector quantization," *IEEE Trans. Commun.*, vol. 36, no. 6, pp. 713-719, June 1988.

[48] P. Westerink, "Subband coding of images," Ph.D. thesis, Delft Univ. of Technol., Delft, The Netherlands, 1989.

[49] K. J. Wong, P. Y. Cheng, and C. C. J. Kuo, "JPEG-based image compression scheme using fully decomposed wavelet packet (FWP) transform," *Proc. SPIE*, vol. 2186, pp. 75-86. 1994.

[50] J. W. Woods and S. D. O'Neil, "Subband coding of images," *IEEE Trans. ASSP*, vol. 34, no. 5, pp. 1278-1288, Oct. 1986.

[51] Y. Yang, N. P. Galatsanos, and A. K. Katsaggelos, "Regularized reconstruction to reduce blocking artifacts of block discrete cosine transform compressed image," *IEEE Trans. Circuits Syst. Video Technol.*, vol. 3, no. 6, pp. 421-432, Dec. 1993.

[52] Y. Yang, N. P. Galatsanos, and A. K. Katsaggelos, "Projection-based spatially adaptive reconstruction of block-transform compressed images," *Proc. SPIE*, vol. 2308, pp. 1477-1488, 1994.

[53] R. Yarlagadda and J. Hershey, "Architecture of the fast Walsh-Hadamard and fast Fourier transforms with charge transfer devices," *Int. J. Electronics*, vol. 51, pp. 669-681, 1981.

[54] R. Yarlagadda and J. Hershey, "A naturalness-preserving transform for image coding and reconstruction," *IEEE Trans. ASSP*, vol. 33, no. 4, pp. 1005-1012, 1985.

[55] R. Yarlagadda and J. Hershey, *Hadamard Matrix Analysis and Synthesis*, Kluwer Academic Publishers, 1997.

[56] D. C. Youla, "Generalized image restoration by the method of alternating orthogonal projections, " *IEEE Trans. Circ. Syst.*, vol. 25, pp. 694-702, Sept. 1978.

[57] D. C. Youla and H. Webb, "Image restoration by the method of convex projections," *IEEE Trans. Med. Imaging*, vol. 1, pp. 81-101, Oct. 1982.

[58] T. H. Yu and S. K. Mitra, "A simple image analysis/synthesis technique and its application in image coding," *Proc. SPIE*, vol. 1244, pp.161-170, 1990.

[59] S. Zhong, "Image smoothing respecting feature direction," *Workshop on Scientific Computing '97*, Hong Kong, 1997.

[60] S. Zhong, "Image coding with optimal reconstruction," *Proc. ICIP '97*, 1997.

APPENDIX A

TEST IMAGES

This appendix provides examples of the 8 bit grayscale images used in this research. *Peppers*, *Zelda*, and *Mandrill* are 512 x 512 images. The remaining images are 256x256. The *A256* and *C256* images were provided by Sandia National Labs.
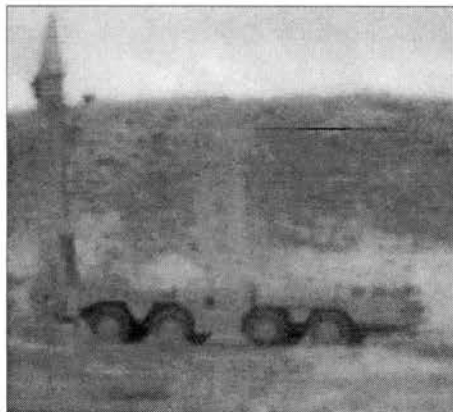
A256

C256

Cameraman
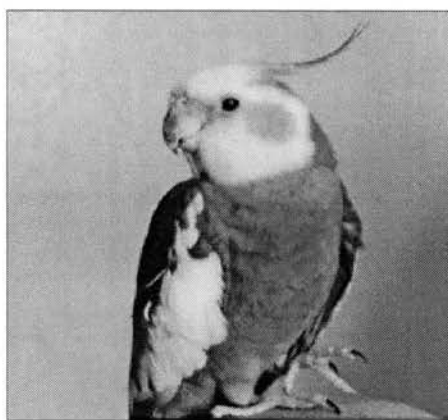
Bird

Bridge

Lena

Goldhill

Peppers

Zelda
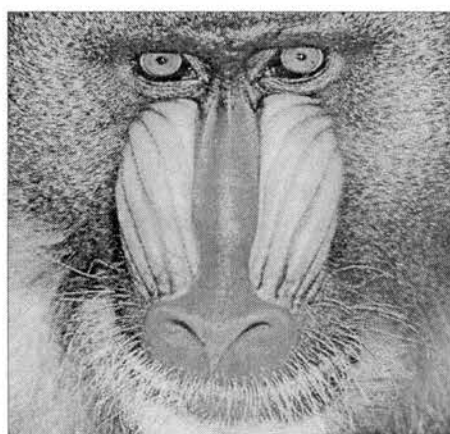
Mandrill

APPENDIX B

QUANTIZATION TABLES

This appendix lists the quantization tables used for the compression examples given in Chapter 4 of this paper. Symmetric Lloyd-Max quantizers were designed for the Gamma probability density function (Equation (4.3)) with a shape parameter value equal to $\gamma = 0.5$ or $\gamma = 0.6$. Both the decision and reconstruction levels are listed for each quantizer. Because the quantizers are symmetric, each table lists only the absolute value of each level.

γ = 0.5 Number of Levels Distortion	3 0.2939		4 0.2232		5 0.1377		6 0.1131	
	x_k	y_k	x_k	y_k	x_k	y_k	x_k	y_k
	.9256	1.850	1.300	2.255	2.030	3.024	2.317	3.321
		0.000	0.000	0.345	0.519	1.037	0.772	1.313
						0.000	0.000	0.230

γ = 0.5 Number of Levels Distortion	7 0.0813		8 0.0695		15 0.0211		16 0.0187	
	x_k	y_k	x_k	y_k	x_k	y_k	x_k	y_k
	2.879	3.905	3.113	4.146	5.018	6.083	5.011	6.026
	1.282	1.853	1.500	2.080	3.334	3.952	3.393	3.995
	0.355	0.710	0.545	0.919	2.285	2.715	2.367	2.791
		0.000	0.000	0.171	1.530	1.854	1.623	1.944
					0.951	1.205	1.049	1.302
					0.497	0.698	0.594	0.796
					0.149	0.297	0.235	0.391
						0.000	0.000	0.078

γ = 0.5 Number of Levels Distortion	31 0.0054		32 0.0052	
	x_k	y_k	x_k	y_k
	7.242	8.328	7.312	8.399
	5.517	6.155	5.586	6.224
	4.429	4.880	4.497	4.948
	3.632	3.979	3.699	4.046
	3.005	3.286	3.071	3.352
	2.490	2.724	2.555	2.790
	2.055	2.255	2.119	2.320
	1.680	1.854	1.743	1.917
	1.353	1.506	1.414	1.568
	1.065	1.200	1.124	1.260
	0.810	0.930	0.867	0.988
	0.583	0.690	0.638	0.746
	0.383	0.477	0.435	0.530
	0.208	0.289	0.256	0.339
	0.064	0.128	0.105	0.173
		0.000	0.000	0.036

$\gamma = 0.5$ Number of Levels Distortion	63 0.0014		64 0.0013	
	x_k	y_k	x_k	y_k
	9.525	10.625	9.558	10.658
	7.777	8.426	7.810	8.458
	6.669	7.129	6.701	7.161
	5.852	6.209	5.885	6.241
	5.206	5.496	5.238	5.528
	4.672	4.916	4.703	4.948
	4.216	4.427	4.248	4.459
	3.820	4.006	3.852	4.037
	3.471	3.635	3.502	3.667
	3.158	3.306	3.189	3.337
	2.875	3.009	2.906	3.040
	2.617	2.740	2.648	2.771
	2.380	2.494	2.411	2.525
	2.162	2.267	2.193	2.298
	1.960	2.058	1.991	2.088
	1.772	1.863	1.802	1.893
	1.597	1.682	1.627	1.712
	1.432	1.512	1.462	1.542
	1.278	1.353	1.308	1.382
	1.133	1.204	1.163	1.233
	0.997	1.063	1.026	1.092
	0.869	0.931	0.897	0.960
	0.748	0.806	0.776	0.834
	0.634	0.689	0.661	0.717
	0.526	0.578	0.553	0.605
	0.425	0.474	0.452	0.501
	0.331	0.377	0.357	0.403
	0.243	0.286	0.268	0.311
	0.163	0.201	0.186	0.225
	0.090	0.124	0.111	0.147
	0.028	0.056	0.046	0.076
		0.000	0.000	0.016

$\gamma = 0.6$ Number of Levels Distortion	3 0.2879		4 0.2127		5 0.1341		6 0.1080	
	x_k	y_k	x_k	y_k	x_k	y_k	x_k	y_k
	0.858	1.715	1.240	2.123	1.884	2.793	2.175	3.093
	0.000		0.000	0.358	0.487	0.975	0.750	1.257
						0.000	0.000	0.243

$\gamma = 0.6$ Number of Levels Distortion	7 0.0779		8 0.0659		15 0.0202		16 0.0181	
	x_k	y_k	x_k	y_k	x_k	y_k	x_k	y_k
	2.658	3.589	2.890	3.827	4.593	5.552	4.662	5.600
	1.200	1.726	1.421	1.954	3.075	3.635	3.172	3.725
	0.337	0.674	0.535	0.888	2.124	2.516	2.230	2.619
		0.000	0.000	0.183	1.435	1.732	1.544	1.841
					0.902	1.137	1.011	1.247
					0.478	0.667	0.583	0.774
					0.145	0.290	0.240	0.392
						0.000	0.000	0.088

$\gamma = 0.6$ Number of Levels Distortion	31 0.0051		32 0.0049	
	x_k	y_k	x_k	y_k
	6.596	7.569	6.662	7.636
	5.050	5.623	5.116	5.689
	4.071	4.477	4.137	4.543
	3.353	3.666	3.417	3.731
	2.785	3.040	2.849	3.104
	2.318	2.531	2.381	2.595
	1.922	2.104	1.984	2.168
	1.579	1.739	1.641	1.801
	1.279	1.420	1.340	1.481
	1.013	1.138	1.072	1.198
	0.776	0.888	0.833	0.946
	0.563	0.664	0.620	0.721
	0.374	0.463	0.428	0.519
	0.206	0.285	0.258	0.338
	0.064	0.128	0.109	0.178
		0.000	0.000	0.041

$\gamma = 0.6$				
Number of Levels	63		64	
Distortion	0.0013		0.0013	
	x_k	y_k	x_k	y_k
	8.641	9.623	8.675	9.658
	7.079	7.659	7.113	7.693
	6.086	6.499	6.120	6.533
	5.354	5.674	5.388	5.708
	4.774	5.035	4.808	5.068
	4.293	4.513	4.327	4.547
	3.884	4.074	3.917	4.107
	3.527	3.694	3.560	3.727
	3.210	3.359	3.243	3.392
	2.927	3.062	2.960	3.094
	2.671	2.793	2.703	2.826
	2.437	2.549	2.469	2.581
	2.222	2.325	2.254	2.357
	2.023	2.119	2.055	2.151
	1.839	1.928	1.870	1.960
	1.667	1.750	1.698	1.781
	1.506	1.584	1.537	1.615
	1.355	1.428	1.386	1.459
	1.213	1.281	1.243	1.313
	1.079	1.144	1.109	1.174
	0.952	1.014	0.986	1.044
	0.833	0.891	0.863	0.921
	0.720	0.775	0.749	0.805
	0.613	0.665	0.642	0.694
	0.512	0.561	0.540	0.590
	0.416	0.463	0.444	0.491
	0.326	0.370	0.354	0.398
	0.242	0.283	0.269	0.310
	0.164	0.201	0.189	0.227
	0.092	0.126	0.116	0.151
	0.029	0.058	0.050	0.080
		0.000	0.000	0.019

$\sqrt{}$

VITA

Charlotte Renee Fore

Candidate for the Degree of

Doctor of Philosophy

Thesis: COMPRESSION AND RECONSTRUCTION OF HADAMARD
NATURALNESS-PRESERVING TRANSFORM CODED IMAGES

Major Field: Electrical Engineering

Biographical:

Personal Data: Born in Stillwater, Oklahoma, on March 5, 1967, the daughter of
Raymond F. and Lanora Heiser.

Education: Received Bachelor of Science degree in Physics from Oral Roberts
University, Tulsa, Oklahoma in May 1989; received Master of Science
degree in Electrical Engineering from Oklahoma State University,
Stillwater, Oklahoma in July 1993; Completed the requirements for the
Doctor of Philosophy degree at Oklahoma State University in May, 1999.

Professional Experience: Teaching Assistant, Department of Physics, Oklahoma
State University, from August 1989 to May 1990; Teaching Assistant,
School of Electrical and Computer Engineering, Oklahoma State
University, from August 1990 to May 1993; Graduate Research Assistant,
School of Electrical and Computer Engineering, Oklahoma State
University, from June 1993 to present.